Copyright Warning & Restrictions

The copyright law of the United States (Title 17, United States Code) governs the making of photocopies or other reproductions of copyrighted material.

Under certain conditions specified in the law, libraries and archives are authorized to furnish a photocopy or other reproduction. One of these specified conditions is that the photocopy or reproduction is not to be "used for any purpose other than private study, scholarship, or research." If a, user makes a request for, or later uses, a photocopy or reproduction for purposes in excess of "fair use" that user may be liable for copyright infringement,

This institution reserves the right to refuse to accept a copying order if, in its judgment, fulfillment of the order would involve violation of copyright law.

Please Note: The author retains the copyright while the New Jersey Institute of Technology reserves the right to distribute this thesis or dissertation

Printing note: If you do not wish to print this page, then select "Pages from: first page # to: last page #" on the print dialog screen

ABSTRACT

ADAPTIVE SPACE-TIME PROCESSING FOR WIRELESS COMMUNICATIONS

by
Xiao Cheng Bernstein

Adaptive space-time processing techniques have been found to increase the capacity of two major, multiple-access wireless communication systems: Time Division Multiple Access (TDMA) and Code Division Multiple Access (CDMA).

In an IS-54 TDMA system, the frequency re-use factor has to be set to 7 so that cells with the same spectrum are separated far enough to meet a required carrier-to-interference ratio (CIR). Space processing uses multiple antennas which, in turn, provide alternative signal paths in order to cancel interferences and combat multipath fading. We have proposed the *eigencanceler* method and have reviewed the theoretical optimum combining and the feasible *direct matrix inverse* (DMI) technique. An analysis of the system performance reveals that when data sets are small, the eigencanceler is superior to DMI. Furthermore, we have proposed a simple projection-based algorithm and have analyzed its performance.

The capacity of CDMA communication systems is restricted by multiple-access interferences (MAI). We have shown that spatial and temporal processing can be combined to increase the capacity of CDMA-based wireless communications systems. The degrees of freedom provided by space-time processing can be exploited to combat both fading and MAI. Specifically, we have discussed the following methods: (1) space-time diversity, (2) cascade optimum spatial-diversity temporal, (3) cascade optimum spatial-optimum temporal, and (4) joint-domain optimum processing. We have proved that, due to its interference cancellation capability, *optimum combining* provides significantly better performance than diversity techniques.

ADAPTIVE SPACE-TIME PROCESSING FOR WIRELESS COMMUNICATIONS

by
Xiao Cheng Bernstein

A Dissertation
Submitted to the Faculty of
New Jersey Institute of Technology
in Partial Fulfillment of the Requirements for the Degree of
Doctor of Philosophy

Department of Electrical and Computer Engineering

January 1996

APPROVAL PAGE

ADAPTIVE SPACE-TIME PROCESSING FOR WIRELESS COMMUNICATIONS

Xiao Cheng Bernstein

Dr. Alexander M. Haimovich, Dissertation Advisor — Date
Associate Professor of Electrical and Computer Engineering, NJIT

Dr. Yeheskel Bar-Ness, Committee Member — Date
Distinguished Professor of Electrical and Computer Engineering, NJIT

Dr. Michael Porter, Committee Member — Date
Professor of Mathematics, NJIT

Dr. Zoran Siveski, Committee Member — Date
Assistant Professor of Electrical and Computer Engineering, NJIT

Dr. Jack H. Winters, Committee Member — Date
Member of Technical Staff, AT&T Bell Laboratories, Holmdel, NJ

BIOGRAPHICAL SKETCH

Author: Xiao Cheng Bernstein

Degree: Doctor of Philosophy

Date: January 1996

Undergraduate and Graduate Education:

- Doctor of Philosophy in Electrical Engineering,
  New Jersey Institute of Technology, Newark, NJ, 1996
- Master of Science in Electrical Engineering,
  Shanghai Jiao Tong University, Shanghai, P. R. China, 1991
- Bachelor of Science in Electrical Engineering,
  Shanghai Jiao Tong University, Shanghai, P. R. China, 1988

Major: Electrical Engineering

Presentations and Publications:

Xiao C. Wu and Alexander M. Haimovich,
"Adaptive arrays for increased performance in mobile communications,"
The Sixth International Symposium on Personal, Indoor and Mobile Radio Communications (PIMRC'95), Toronto, Canada, September 1995.

Xiao C. Wu and Alexander M. Haimovich,
"Space-time processing for CDMA communications,"
Proceedings of the 1995 Conference on Information Science and Systems, Baltimore, MD, pp. 371-376, March 1995.

Xiao C. Wu and Alexander M. Haimovich,
"A simple projection based adaptive array with applications to mobile communications,"
Proceedings of the 1994 Adaptive Antenna Systems Symposium, Melville, NY, pp. 37-42, November 1994.

To my beloved family

ACKNOWLEDGMENT

I would like to express my deepest appreciation to Dr. Alexander Haimovich, who not only served as my research supervisor, providing valuable and countless resources, insight, and intuition, but also constantly gave me support, encouragement, and reassurance. Special thanks are given to Dr. Yeheskel Bar-Ness, Dr. Zoran Siveski, Dr. Michael Porter and Dr. Jack Winters for actively participating in my committee.

Many of my fellow graduate students in the Communications and Signal Processing Research Center are deserving of recognition for their support. I also wish to thank Lisa Fitton for her assistance over the years.

TABLE OF CONTENTS

TABLE OF CONTENTS
(Continued)

LIST OF TABLES

LIST OF FIGURES

LIST OF FIGURES
(Continued)

CHAPTER 1

INTRODUCTION

1.1 Objective

The objective of this dissertation is to present applications of space-time processing for the following multiple-access, wireless communication systems: time-division multiple-access (TDMA) and code-division multiple-access (CDMA).

For the TDMA system, we review the following spatial processing techniques: *optimum combining* and *direct matrix inverse* (DMI); and we propose eigenanalysis-based processing, or the *eigencanceler*. An analysis of system performance shows that the eigencanceler is superior to DMI when small data sets are available. Also, a simple algorithm implementing the eigencanceler is proposed and its performance is analyzed. This algorithm is compared with (1) the least-mean-square (LMS) algorithm, (2) recursive least-squares (RLS) algorithm, and (3) the power method.

For the CDMA system, the following receiver configurations are formulated and compared: (1) space-time *maximum ratio combining* (SMRC/TMRC) (in effect space-time diversity), (2) cascade optimum space-MRC time (SOPT/TMRC) (optimum spatial processing cascaded with a RAKE receiver), (3) cascade optimum space-optimum time (SOPT/TOPT), and (4) joint domain optimum combining (JOPT). It is shown that by upgrading from the SMRC/TMRC receiver to optimum combining significant capacity improvements can be achieved. The best performance is shown with the JOPT receiver. By increasing the number of antennas from one to two, the capacity increases by at least 100%.

1.2 Background Information

Wireless communication offers universal network access by removing users' location and time constraints. As wireless networks proliferate and the subscriber community continues to expand rapidly, there is an increasing demand for the development of

spectrally efficient multiple-access schemes to alleviate spectral congestion. State-of-the art technology already allows the deployment of some multiple-access systems, while active research is ongoing to improve the performance of future systems [4, 19, 6]. The main objective of the research is to increase network capacity without impairing service [8].

There are three types of multiple-access schemes based on a frequency, time and code division multiple-access referred to as FDMA, TDMA and CDMA, respectively. The "first-generation" cellular systems use the FDMA scheme for spectrum sharing, analog *frequency modulation* (FM) for speech transmission, and *frequency shift keying* (FSK) for signaling. The *advanced mobile phone system* (AMPS), developed by AT&T for the USA, and the *total access communication system* (TACS), used in the UK and a number of other countries, belong to the "first-generation." In these cellular systems, each cell is allocated a set of frequencies. Interference between cells is minimized by assigning different frequency bands to neighboring cells. Frequencies are reused at intervals one or two cells apart. Demand for increased capacity in a certain area can be satisfied by cell splitting. A degree of the splitting, however, is limited by the overhead of handoffs between cells.

The "second-generation" cellular systems are entirely digital. This allows TDMA and CDMA to be feasible. The TDMA system adds time slots on each radio channel, thus allowing more users to share the same spectrum. The *global system for mobile communications* (GSM), specified by the European Telecommunications Standards Institute (ETSI), as well as IS-54, adopted by the Electronic Industries Association (EIA) and Telecommunications Industry Association (TIA) in North America, are TDMA cellular systems. TDMA system capacity can be further increased by using spatial processing (antenna arrays). CDMA, as a spread spectrum system, has distinct advantages over FDMA and TDMA systems. It has a larger capacity than either FDMA or TDMA. The IS-95 CDMA standard is adopted by

the EIA/TIA in North America. Multipath fading and multiple-access interference (MAI), however, limit the CDMA system's capacity. Antenna arrays, combined with temporal processing could provide a cost efficient means to increase the capacity of the CDMA system.

The frequency re-use factor determines the number of cells that share an entirely allocated spectrum. Reduction of the frequency re-use factor can increase system capacity. None of the existing standard TDMA systems, however, can reach the lowest frequency reuse factor of 1, because the low frequency re-use factor results in high interference power, which in turn degrades the system performance. In the IS-54 TDMA system, the frequency re-use factor has to be set to 7 so that cells with the same spectrum are separated far enough to meet the required *carrier-to-interference ratio* (CIR). Space processing employs multiple antennas to provide alternative signal paths to cancel interferences and combat multipath fading so that it can reduce the required CIR. An adaptive array exploits the correlation between the interference signals at the array elements to steer nulls in their direction. Winters [33] studied the application of an adaptive array at the base station to maximize the *signal-to-noise-plus-interference ratio* (SNIR). He assumed a flat Rayleigh fading channel and independent fading between antennas and found a Wiener filter solution for the optimal weight-vector. Also, he showed that an antenna array may allocate available degrees of freedom either to null interferences or for path diversity to combat fading [35]. Additional applications of adaptive arrays to co-channel interference cancellation in mobile communications, can be found in refs. [27, 30]. The number of antennas is restricted by the available data size, for instance by a 14-symbol synchronization sequence as in IS-54 system. Thus, a suboptimum combining scheme, which converges with a small data size, is of particular interest.

In ref. [11], we proposed an eigenanalysis-based technique for spatial filtering of co-channel interferences. Originally applied to spectral estimation and direction-

finding problems, the eigenstructure of the received data correlation matrix can also be exploited for developing an adaptive filter [10]. This filter, referred to as the eigencanceler, was found to perform particularly well when only a few samples are available for estimating the correlation matrix. The eigenanalysis-based adaptive array is being applied to the flat Rayleigh, slowly fading channel, which in turn characterizes the mobile communications environment. In this dissertation, the eigencanceler's performance with respect to rejection of co-channel interference is compared with, and shown to be superior to DMI method. Further implementation of the eigencanceler has been suggested by applying a simple projection-based algorithm for updating the signal space decomposition and computing the weight-vector. The algorithm has an $O(Nr^2)$ complexity, where N is the dimension of the matrix and r is the rank of the interference subspace. The algorithm is shown to be faster than the LMS adaptive algorithm for optimum combining and its speed is comparable to the RLS. The tracking ability is also simulated in this dissertation and compared to [34].

As a result of extensive research over the last few years, cellular CDMA has emerged as an attractive alternative to the veteran FDMA and to TDMA. CDMA has been shown to be particularly advantageous in terrestrial digital cellular systems [20, 14], and it could become the long term answer to personal communication systems (PCS). Its capabilities stem from the specifics of the environment encountered in wireless PCS. In a typical urban environment the signal delay spread corresponds to a coherence bandwidth of the order of a few hundred kilohertz. The IS-95 standard defines the CDMA signal with a bandwidth of 1.25 MHz. This bandwidth is typically several times larger than the channel coherence bandwidth encountered by the systems, and thus it provides for path diversity, which can be exploited to mitigate multipath effects. CDMA signals are overlaid in the frequency channel and are separated based on their waveform signature. Consequently, it is possible to reuse

the entire spectrum in each cell (re-use factor of 1). Such a scheme can inherently take advantage of low voice activity since, with respect to any particular user, the interference is formed by the aggregate of the other signals. The performance of CDMA-based systems is ultimately limited by co-channel interference, thus it is said to be interference limited.

If the transmissions from the base station are synchronized, a judicious choice of codes can minimize interferences at the mobile downlink (site-to-mobile). On the uplink, however, signals use different propagation paths and even with synchronization, the users' signals cannot be made orthogonal, making CDMA vulnerable to *near-far* effects. Due to non-zero cross-correlations between waveforms, strong signals from closer users may have a deleterious effect on the designated user's signal. This problem can be mitigated using power control. To be effective, however, the power control needs to be accurate (typically within 1 dB), be fast and have a large dynamic range [19]. The quality of power control has been shown to have a great impact on the performance of CDMA systems [32]. Near-far effects are exacerbated by the multipath fading and shadowing environment typical in urban PCS environments. The multipath fading problem is mitigated by the use of the RAKE receiver, which constructively combines the resolved signal paths.

A further increase in the capacity of CDMA-based wireless communication systems is possible by exploitation of the spatial domain in the transmit or receive mode [40, 31, 21]. There are several ways in which an antenna array could operate in a wireless communication system. If line-of-sight is available, multiple transmit/receive beams could be formed at the base station. Generation of multiple transmit beams involves either parallel transmit modules or beam agility. Either way, multiple transmit beams are a complex and expensive solution. Beamforming on receiver is easier to accomplish since it can be implemented digitally or even in software. Classical beamforming forms narrow beams in specified directions. However, in an

urban environment affected by severe multipath, the line-of-sight scenario is not likely. Thus a generalized form of beamforming is required, in which beams are not associated with physical directions, but rather with a propagation vector representing the aggregate of all the propagation paths resulting from a specific source. The viewpoint adopted in this paper is that of the single user, with the tacit assumption that in a multiuser application, the solutions discussed need to be replicated for the other users. A rudimentary form of arrays (sector antennas) have been incorporated in second-generation wireless cellular systems. The arrangement provides directivity in specified sectors, but the patterns are designed for no overlap. Hence, spatial/temporal correlations cannot be exploited. Unlike sector antennas, in an adaptive array, individual antenna patterns overlap and signal processing can be brought to bear to improve performance. As an interest in the CDMA systems grows, there is an increasing number of publications considering the benefits of antenna arrays to CDMA-based systems. A co-channel interference canceler based on null-steering is suggested in refs. [18, 17]. The channel model assumed is line-of-sight and a multi-user receiver is used to cancel co-channel interferences at the same angle of arrival as the desired source. An alternative point of view to combining the paths is that of equalizing the channel. In ref.[13], the no distortion Nyquist criterion is extended to the spatial domain and is used to develop zero forcing and minimum mean square error equalizers. In ref. [23], a space-time configuration that consists of an antenna array and a RAKE receiver is suggested. The array and the RAKE receiver are cascaded. Calibration issues for this arrangement are considered in ref. [15]. Further improvement is possible by considering optimum processing in both the space and time domains, either cascaded or jointly.

CHAPTER 2
SPATIAL PROCESSING FOR TDMA SYSTEMS

This chapter demonstrates applications of adaptive array techniques to improve the performance and increase the capacity of TDMA systems. The adaptive array theory is well understood and documented [22]. Applications, however, were slow to exploit this body of knowledge, due to costs of building arrays and high demands on the real-time computing power usually associated with array processing. Nevertheless, conditions may be right for the use of adaptive antennas in mobile communications. Technological advances lowered the cost of hardware and computing power to the point that adaptive antennas have become viable alternatives to other network expansion techniques, such as microcells. The cost of the added complexity may well be offset by increased revenues from expanding traffic and customer base. Furthermore, significant improvement can be achieved even with relatively few antennas and without an undue increase in complexity.

In contrast to traditional array processing, in which antennas are placed at half-wavelength or at smaller intervals such that a high correlation exists between signals across the array, spatial diversity is achieved by placing the antennas at larger intervals to provide for independent signal paths. Signal enhancement is then provided by *maximum ratio combining* (MRC), where each antenna output is weighted proportionally to the signal strength in that channel [24]. MRC combats fading by maximizing the signal-to-noise ratio (SNR) under the assumption of white gaussian noise, i.e. in the absence of co-channel interference. *Optimum combining* has been shown to provide both signal enhancement and interference cancellation [33]. One of the important results in this field is that, under an assumption of slow independent Rayleigh fading, an N-element array can null out L spatial interferences and provide $N-L$ diversity paths [36]. A well known result in array processing is that when the array covariance matrix is estimated from the data, the sample support is

required to be at least twice the array dimension to provide an output SNR within 3 dB of the optimal. The 14-symbol synchronization sequence provided by the IS-54 standard, could be used for array training. Due to the limited sample support, fast adaptive techniques which might outperform DMI are of particular interest.

In mobile communications, the signal environment varies due to the motion of the mobiles. However, fast adaptive techniques are of capable of tracking the changing signals. This is yet another reason why fast adaptive techniques are of great interest [34]. In ref. [11], we have proposed the eigencanceler method. The eigencanceler is derived from the decomposition of the signal space into interference and noise subspaces, and the construction of a weight vector in the noise subspace [10]. In this chapter, we show that the eigencanceler can perform particularly well with small data sets.

Section 2.1 presents the problem statement and the conventional Wiener filter for interference suppression. In Section 2.2, the eigencanceler is formulated. Its performance is evaluated by analysis and simulations in Section 2.3 and Section 3.3, and conclusions are summarized in Section 2.6.

2.1 Problem Statement

Consider a mobile communication system in which mobiles communicate with the base station. The base station consists of an N-element antenna array. The signals are assumed to be narrowband, hence they can be represented by samples of their complex envelopes. We assume the channel is characterized by flat Rayleigh fading, independent between the antennas. The fading is assumed fixed over the processing interval and independent between processing intervals. If the multipath delay is larger than one tenth of a symbol duration, it may cause intersymbol interference, which can be equalized using a tap-delay line filter at each antenna. In this paper, however, we emphasize spatial processing. Hence, the delay spread is assumed small

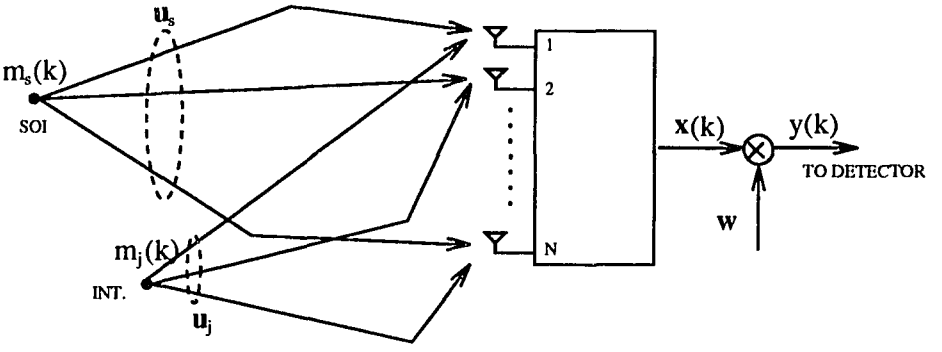

Figure 2.1 Adaptive array

so that a single weight at each antenna is sufficient. Let $\mathbf{x}(k)$ be the $N \times 1$ data vector of antenna outputs at time $t = kT$, where T is the symbol interval. As shown in Figure 2.1, the data vector consists of contributions of the signal-of-interest (SOI) $\mathbf{x}_s(k)$, co-channel interferences due to the other users' signals $\mathbf{x}_j(k)$, $j = 1, \ldots, L$, and samples of white complex Gaussian noise $\mathbf{v}(k)$, with a zero mean and a variance equal to $\sigma^2 = N_o/T$:

$$\mathbf{x}(k) = \mathbf{x}_s(k) + \sum_{j=1}^{L} \mathbf{x}_j(k) + \mathbf{v}(k) \tag{2.1}$$

With the fading model assumed, each source (SOI or interference) may be represented by a propagation vector $\mathbf{u}$, whose components are realizations of independent, complex Gaussian random variables with zero means, and unit variances. This model implies that the array elements are sufficiently separated to allow independent fading between antennas. The vector $\mathbf{x}(k)$, can be written as:

$$\mathbf{x}(k) = m_s(k)A_s\mathbf{u}_s + \sum_{j=1}^{L} m_j(k)A_j\mathbf{u}_j + \mathbf{v}(k) \tag{2.2}$$

where $m_s(k)$, $m_j(k)$ are complex data symbols, $A_s = \sqrt{E_s/T}$ and $A_j = \sqrt{E_j/T}$ are the amplitudes, and $\mathbf{u}_s$ and $\mathbf{u}_j$ are the propagation vectors of the SOI and inter-

ferences, respectively. E_s and E_j are the received signal energy per symbol of the SOI and interferences, respectively.

With slow fading, we assume that the interference-plus-noise correlation matrix is stationary over the processing time and define

$$\mathbf{R}_n = \mathrm{E}\left[\mathbf{x}_n(k)\mathbf{x}_n^H(k) \mid \mathbf{u}_j\right], \tag{2.3}$$

where the superscript $(.)^H$ denotes the complex conjugate transpose and $\mathbf{x}_n(k) = \mathbf{x}(k) - \mathbf{x}_s(k)$ is the interference-plus-noise data vector. The expectation is taken with respect to the noise and conditioned on the values of the propagation vectors $\mathbf{u}_j$, $j = 1, \ldots, L$. The weight vector that maximizes the SNIR is given by the well-known relation:

$$\mathbf{w}_o = c\mathbf{R}_n^{-1}\mathbf{r}_{sx}, \tag{2.4}$$

where c is a scaling constant and $\mathbf{r}_{sx}$ is the cross-correlation vector defined as $\mathbf{r}_{sx} = \mathrm{E}[m_s^*(k)\mathbf{x}(k) \mid \mathbf{u}_s]$. Note that $\mathbf{r}_{sx} = \mathrm{E}[m_s(k)\mathbf{x}(k) \mid \mathbf{u}_s] = A_s\mathbf{u}_s$. The processor in equation (2.4) is referred to as the *optimal combiner*. The output of the optimal combiner is constructed as $y(k) = \mathbf{w}_o^H\mathbf{x}(k)$, which is the input of the detector.

The statistics of the received signal channels typically are not known and, furthermore, will vary over time. This is why adaptive methods are required to track the signal environment. Methods for estimating the weight vector, when the statistics of the data are not known, are commonly classified as either block processing or adaptive processing. With block processing, the correlation matrix and cross-correlation vector are estimated from a block of received data. With adaptive processing, the new data is used directly to update the weight vector. The weight vector calculation based on block processing is known as the direct matrix inversion (DMI) method [26]:

$$\mathbf{w} = \widehat{\mathbf{R}}_n^{-1}\hat{\mathbf{r}}_{sx}, \tag{2.5}$$

where the estimated correlation matrix $\widehat{\mathbf{R}}_n = \frac{1}{K}\sum_{k=1}^{K} \mathbf{x}_n(k)\mathbf{x}_n^H(k)$ and the estimated cross-correlation vector $\widehat{\mathbf{r}}_{sx} = \frac{1}{K}\sum_{k=1}^{K} m_s^*(k)\mathbf{x}(k)$ are obtained from averages over K data vectors. The estimation process results in a performance loss with respect to the case of known statistics.

The Wiener filter provides the optimal solution when data statistics are stationary and known. When the statistics are estimated from the data the solution is not necessarily optimal and is affected by the quality of the estimates. In particular, it has been shown that when the signal $\mathbf{x}_n(k)$ is Gaussian, $\widehat{\mathbf{R}}_n$ has a Wishart distribution and more than $2N$ snapshots are required in order to obtain a solution within 3 dB of the optimal SNIR [26]. In the next section we introduce an eigenanalysis-based array processing technique, which subsequently is shown to converge (i.e. it requires less data for estimation) much faster than the Wiener filter, when the number of interferences is limited.

2.2 Eigenanalysis Filter

The eigenanalysis-based filter is developed from properties suggested by the eigendecomposition of the array correlation matrix [11]. Consider the interference-plus-noise correlation matrix $\mathbf{R}_n = \sum_{j=1}^{L} P_j \mathbf{u}_j \mathbf{u}_j^H + \sigma_v^2 \mathbf{I}$. When the number of interferences L is less than the number of antennas in the array N, the L propagation vectors $\mathbf{u}_j$ are usually linearly independent and span a signal subspace, referred to as the *interference subspace.* Assuming interferences are strong, the matrix $\mathbf{U} = \sum_{j=1}^{L} P_j \mathbf{u}_j \mathbf{u}_j^H = \mathbf{R}_x - \sigma_v^2 \mathbf{I}$ has $L < N$ non-zero eigenvalues. The eigenvalues of $\mathbf{R}_n$, $\lambda_i(\mathbf{R}_n)$, are those of $\mathbf{U}$ plus the white Gaussian noise eigenvalues, $\lambda_i(\mathbf{R}_n) = \lambda_i(\mathbf{U}) + \sigma_v^2$, for $i = 1, \ldots, N$. Hence, the L largest eigenvalues of $\mathbf{R}_n$ represent the interference sources. It is well known that the eigenvectors $\mathbf{q}_i$ associated with these eigenvalues span the same algebraic subspace as the interference subspace [12]; namely, span $[\mathbf{q}_1, \ldots, \mathbf{q}_L]$ = span $[\mathbf{u}_1, \ldots, \mathbf{u}_L]$. Hence, the orthogonal complement of

the interference subspace, termed the noise subspace, has the following orthogonality property.

$$\text{span}\left[\mathbf{q}_{L+1},\ldots,\mathbf{q}_N\right] \perp \text{span}\left[\mathbf{u}_1,\ldots,\mathbf{u}_L\right]. \tag{2.6}$$

When the number of interferences $L \geq N$, there is no noise subspace orthogonal to the span $[\mathbf{u}_1,\ldots,\mathbf{u}_L]$. Yet, the total interference-plus-noise power, given by $P_n = \text{trace}[\mathbf{R}_n] = \sum_{i=1}^{N} \lambda_i(\mathbf{R}_n)$, is concentrated in the larger eigenvalues of $\mathbf{R}_n$.

The uneven distribution of the interference power across the eigenvalues of the correlation matrix forms the basis for the eigenanalysis filter. After having defined a partition of the signal space into an r-dimensional interference subspace, $\mathbf{Q}_c = \text{span}[\mathbf{q}_1,\ldots,\mathbf{q}_r]$, and an $(N-r)$-dimensional noise subspace, $\mathbf{Q}_v = \text{span}[\mathbf{q}_{r+1},\ldots,\mathbf{q}_N]$, the eigencanceler is designed as the minimum-norm vector, which is orthogonal to $\mathbf{Q}_c$ and provides a specified gain to the desired signal. The weight vector is then formulated as the solution of the optimization problem:

$$\min_{w} \quad \mathbf{w}^H\mathbf{w} \quad \text{such that} \quad \mathbf{w}^H\mathbf{Q}_c = 0 \quad \text{and} \quad \mathbf{w}^H\mathbf{u}_s = g. \tag{2.7}$$

It can be shown that the solution to (2.7) is given by [10]:

$$\begin{aligned} \mathbf{w}_e &= c_2\left(\mathbf{I} - \mathbf{Q}_c\mathbf{Q}_c^H\right)\mathbf{u}_s \\ &= c_2\mathbf{Q}_v\mathbf{Q}_v^H\mathbf{u}_s, \end{aligned} \tag{2.8}$$

where $c_2 = g\left|\mathbf{Q}_v^H\mathbf{u}_s\right|^{-2}$, and we used the relation $\mathbf{Q}_c\mathbf{Q}_c^H + \mathbf{Q}_v\mathbf{Q}_v^H = \mathbf{I}$.

For $L < N$, the best partition is given by $r = L$. This can be seen by evaluating $\mathbf{w}_e^H\mathbf{w}_e$ for $r = L$ and for $r = L+1$. From relation (2.8) and the value of the constant c_2, we have:

$$\begin{aligned} \mathbf{w}_e^H\mathbf{w}_e(L) &= |g|^2\left(\mathbf{u}_s^H\mathbf{Q}_v\mathbf{Q}_v^H\mathbf{u}_s\right)^{-1} \\ &= \left(\mathbf{u}_s^H\left[\mathbf{q}_L\ \mathbf{Q}_v'\right]\begin{bmatrix}\mathbf{q}_L^H \\ \mathbf{Q}_v'^H\end{bmatrix}\mathbf{u}_s\right)^{-1} \\ &\leq \left(\mathbf{u}_s^H\mathbf{Q}_v'\mathbf{Q}_v'^H\mathbf{u}_s\right)^{-1} \\ &= \mathbf{w}_e^H\mathbf{w}_e(L+1), \end{aligned} \tag{2.9}$$

where $\mathbf{Q}_v'$ denotes the matrix whose columns span the noise subspace for $r = L+1$. Since span $\left[\mathbf{Q}_v'\right] \in$ span $[\mathbf{Q}_v]$, $\mathbf{w}_e(L+1)$ meets the orthogonality condition in (2.6).

Thus, while $\mathbf{w}_e\,(L+1)$ is a solution that meets the constraints, the minimum norm is achieved for $r = L$. Hence, $\mathbf{w}_e\,(L)$ is optimal. When $L \geq N$, the best partition into interference and noise subspaces is not straightforward. Since, as with M, the dimensionality of the interference subspace is increased, there are two conflicting trends: (1) more of the interference is cancelled by including more interference power in the interference subspace, and (2) the gain term $\mathbf{w}_e^H \mathbf{w}_e$ increases due to the restriction of the weight vector to the diminishing noise subspace, resulting in higher noise power. The best partition can be determined empirically from the distribution of the eigenvalues of $\mathbf{R}_n$.

When the correlation matrix is estimated from the data, the eigencanceler's weight vector can be found from the relation:

$$\hat{\mathbf{w}}_e \;=\; c_3 \widehat{\mathbf{Q}}_v \widehat{\mathbf{Q}}_v^H \hat{\mathbf{r}}_{sx}, \tag{2.10}$$

where $\widehat{\mathbf{Q}}_v$ is the estimated noise subspace.

While eigenanalysis-based array processing is suboptimal when the correlation matrix is known, it has distinct advantages over the Wiener solution when the correlation matrix is estimated from the data. This is shown in the next section.

2.3 Performance Evaluation

In this section, analytical expressions are developed for the probability of error of the DMI and the eigenanalysis based methods for the single-interference case [38].

The output SNIR of the optimum combiner, given by

$$\gamma_o \triangleq \mathrm{SNIR}_o = |A_s|^2 \mathbf{u}_s^H \mathbf{R}_n^{-1} \mathbf{u}_s, \tag{2.11}$$

is a random variable dependent on the propagation vectors $\mathbf{u}_s$ and $\mathbf{u}_j$, $j = 1, \ldots, L$. A performance measure independent of the specific fading is the bit error rate (BER) averaged over all fading situations:

$$\text{BER} = \int_0^\infty P_e(\gamma)\, f_\gamma(\gamma) d\gamma, \tag{2.12}$$

where $P_e(\gamma)$ is the probability of error when SNIR equals γ and is determined by a method of modulation. The function $f_\gamma(\gamma)$ is the probability density function (pdf) of output SNIR γ and is determined by fading channel characteristics and adaptive array processing schemes. Although an analytical computation of P_e in the general case is unwieldy, for one interference the average probability of error of the optimum combiner was computed in ref. [33]:

$$\begin{aligned} f_{\gamma_o}(\gamma_o) &= \frac{e^{-\gamma_o \sigma_v^2/|A_s|^2} (\frac{\gamma_o \sigma_v^2}{|A_s|^2})^{N-1} (1 + N\frac{|A_1|^2}{\sigma_v^2})}{\frac{|A_s|^2}{\sigma_v^2}(N-2)!} \\ &\quad \cdot \int_0^1 e^{-(\gamma_o |A_1|^2/|A_s|^2)Nt} (1-t)^{N-2} dt. \end{aligned} \tag{2.13}$$

See appendix A for a detailed calculation of the integral term in equation (2.13). The performance of the optimum combiner, where the covariance matrix is assumed known, provides an upper bound with respect to DMI or eigenanalysis processing.

To simplify the analysis, let us assume that the interference-plus-noise correlation matrix $\mathbf{R}_n$ is estimated, and the cross-correlation vector $\mathbf{r}_{sx}$ is known. The output SNIR of the DMI method based on the estimated interference-plus-noise correlation matrix $\hat{\mathbf{R}}_n$ can be written as:

$$\hat{\gamma}_o \triangleq \text{SNIR}_{\hat{\mathbf{w}}_o} = |A_s|^2 \frac{(\mathbf{u}_s^H \hat{\mathbf{R}}_n^{-1} \mathbf{u}_s)^2}{\mathbf{u}_s^H \hat{\mathbf{R}}_n^{-1} \mathbf{R}_n \hat{\mathbf{R}}_n^{-1} \mathbf{u}_s}. \tag{2.14}$$

The normalized SNIR of the DMI method with respect to the SNIR of the optimum combiner is given by:

$$\rho(\hat{\mathbf{R}}_n) \triangleq \frac{\hat{\gamma}_o}{\gamma_o} = \frac{(\mathbf{u}_s^H \hat{\mathbf{R}}_n^{-1} \mathbf{u}_s)^2}{(\mathbf{u}_s^H \mathbf{R}_n^{-1} \mathbf{u}_s)\mathbf{u}_s^H \hat{\mathbf{R}}_n^{-1} \mathbf{R}_n \hat{\mathbf{R}}_n^{-1} \mathbf{u}_s}. \tag{2.15}$$

The random variable ρ depends on both the channel and the covariance matrix estimate, and is bounded $0 \leq \rho \leq 1$. It was shown by Reed et. al. [16] that the pdf of $\rho(\hat{\mathbf{R}}_n)$ is a Beta-distributed function, which can be written as:

$$f_\rho(\rho) = \frac{K!}{(N-2)!(K+1-N)!}(1-\rho)^{N-2}\rho^{K+1-N}, \tag{2.16}$$

where K represents the number of samples. From eq. 2.16 it is observed that the pdf of ρ is actually independent of the covariance matrix. From the definition in eq. 2.15 $\hat{\gamma}_o = \rho\gamma_o$, hence the pdf of ρ can be expressed conditioned on γ_o, $f_\rho(\rho) = f_\rho(\rho|\gamma_o) = f_\rho(\frac{\hat{\gamma}_o}{\gamma_o}|\gamma_o)$. It follows that the pdf of $\hat{\gamma}_o$ can be found from the expression

$$f_{\hat{\gamma}_o}(\hat{\gamma}_o) = \int_0^\infty \frac{1}{\gamma_o} f_\rho\left(\frac{\hat{\gamma}_o}{\gamma_o}|\gamma_o\right) f_{\gamma_o}(\gamma_o)\, d\gamma_o. \tag{2.17}$$

Combining equations (2.17) and the conditioned probability of error $P_e(e|\gamma)$, the BER for the DMI method can be written as

$$\begin{aligned} \mathrm{BER}_{\mathrm{DMI}} &= \int_0^\infty \frac{1}{\gamma_o} f_{\gamma_o}(\gamma_o)\left[\int_0^{\gamma_o} P_e(\hat{\gamma}_o)\, f_\rho\left(\frac{\hat{\gamma}_o}{\gamma_o}|\gamma_o\right) d\hat{\gamma}_o\right] d\gamma_o & (2.18)\\ &= \int_0^\infty f_{\gamma_o}(\gamma_o)\left[\int_0^1 P_e(\rho\gamma_o)\, f_\rho(\rho)\, d\rho\right] d\gamma_o. & (2.19) \end{aligned}$$

In the case of the eigencanceler, the output SNIR is given by

$$\hat{\gamma}_e \triangleq \mathrm{SNIR}_{\hat{\mathbf{w}}_e} = \frac{\hat{\mathbf{w}}_e^H \mathbf{u}_s \mathbf{u}_s^H \hat{\mathbf{w}}_e}{\hat{\mathbf{w}}_e^H \mathbf{R}_n \hat{\mathbf{w}}_e}. \tag{2.20}$$

The normalized SNIR for the eigencanceler is given by the expression

$$\rho_e(\hat{\mathbf{R}}_n) \triangleq \frac{\hat{\gamma}_e}{\gamma_o} = \frac{(\mathbf{u}_s^H \hat{\mathbf{Q}}_v \hat{\mathbf{Q}}_v^H \mathbf{u}_s)^2}{(\mathbf{u}_s^H \mathbf{R}_n^{-1} \mathbf{u}_s)\,(\mathbf{u}_s^H \hat{\mathbf{Q}}_v \hat{\mathbf{Q}}_v^H \mathbf{R}_n \hat{\mathbf{Q}}_v \hat{\mathbf{Q}}_v^H \mathbf{u}_s)}. \tag{2.21}$$

The pdf of ρ for the eigencanceler has been determined in ref. [9], and is given by

$$f_{\rho_e}(\rho_e) = \frac{K^{r/2}}{2^{r/2}\Gamma(r/2)}(1-\rho_e)^{r/2-1} e^{-K(1-\rho_e)/2}, \tag{2.22}$$

where $\Gamma(.)$ is the standard gamma function and r is the dimension of the interference subspace. Similar to eqs. (2.18) (2.19), the BER for the eigencanceler can be found as

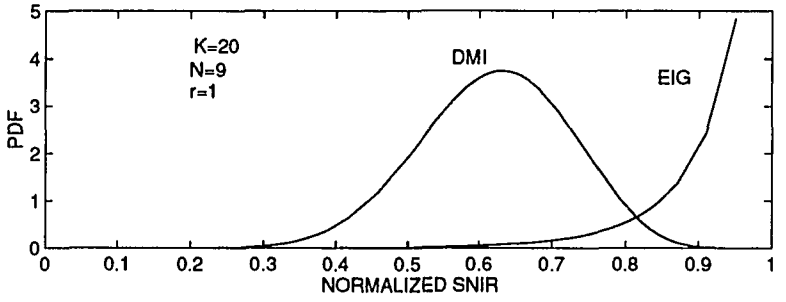

Figure 2.2 The pdf of ρ for N=9

$$\mathrm{BER}_{\mathrm{EIG}} = \int_0^\infty \frac{1}{\gamma_o} f_{\gamma_o}(\gamma_o) \left[\int_0^{\gamma_o} P_e(\hat{\gamma}_e)\, f_{\rho_e}\left(\frac{\hat{\gamma}_e}{\gamma_o} | \gamma_o \right) d\hat{\gamma}_e \right] d\gamma_o \qquad (2.23)$$

$$= \int_0^\infty f_{\gamma_o}(\gamma_o) \left[\int_0^1 P_e(\rho_e \gamma_o)\, f_{\rho_e}(\rho_e)\, d\rho_e \right] d\gamma_o. \qquad (2.24)$$

Although it is difficult to find a closed-form of BER for the case of more than one interference, we can still compare the performance of DMI and the eigencanceler by studying their pdf of ρ. Figure 2.2 shows the pdf of ρ for an N=9 element array and K=20 samples.

For the general case, when both the covariance matrix and the cross-correlation vector are unknown and are estimated from the data, it is very difficult to find a closed-form expression for the pdf of the normalized SNIR ρ. When the input SNR $\gg$ 1, however, the pdf of the normalized SNIR for the DMI method is represented by the expression for a known cross-correlation vector, equation (2.17), substituting $N+1$ for N [22]. Hence, the performance of an N-element array with an unknown $\mathbf{r}_{sx}$ is approximately the same as the performance of an $N-1$ array with a known $\mathbf{r}_{sx}$.

2.4 Numerical Results for the BPSK System

Figure 2.3 shows the BER as a function of the input desired signal SNR for optimum combining, DMI and the eigencanceler with one interference, and assuming BPSK modulation, such that

$$P_e(\gamma) = \frac{1}{2}\,\mathrm{erfc}(\sqrt{\gamma}). \tag{2.25}$$

The SNR at each element is defined as

$$\mathrm{SNR} = \frac{|A_s|^2\,\mathrm{E}\left[|u_{sn}|^2\right]}{\sigma^2} \quad n = 1, \ldots, N, \tag{2.26}$$

where the expectation is over the components of the SOI random propagation vector. The interference-to-noise ratio (INR) at each element is defined as:

$$\mathrm{INR} = \frac{|A_j|^2\,\mathrm{E}\left[|u_{jn}|^2\right]}{\sigma^2} \quad n = 1, \ldots, N;\ j = 1, \ldots, L. \tag{2.27}$$

We set INR=2 dB. The analytical results are shown for several values of N and K. With the sample size K=20, Figure 2.3(a) indicates that with the eigenanalysis-based method and for a probability of bit error of 10^{-3}, N=5 antennas provides a margin of 1 dB SNR over the DMI method; for N=9 this margin increases to 3 dB SNR. When the sample size increases to K=50, as shown in Figure 2.3(b), the margin between the eigencanceler and DMI methods is reduced. The eigencanceler, however, still provides BER curves closer to the optimum bound than does the DMI method. Therefore the eigenanalysis-based method results in superior performance when the estimation is based on short data records.

Figure 2.4 shows the simulation results and theory predictions for the N=9, K=20 and INR=2 dB case. The simulation results nearly match the theory predictions. The precision of the theory predictions depends on the size of integral region. Since the tails of the SNIR pdf functions are cut off, the offset always shows that the simulation results are slightly better than the theory predictions.

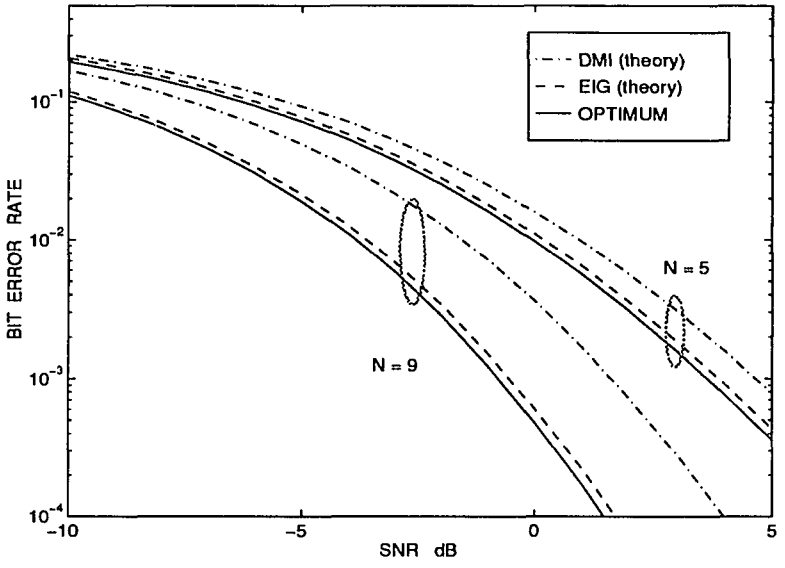

(a) K=20

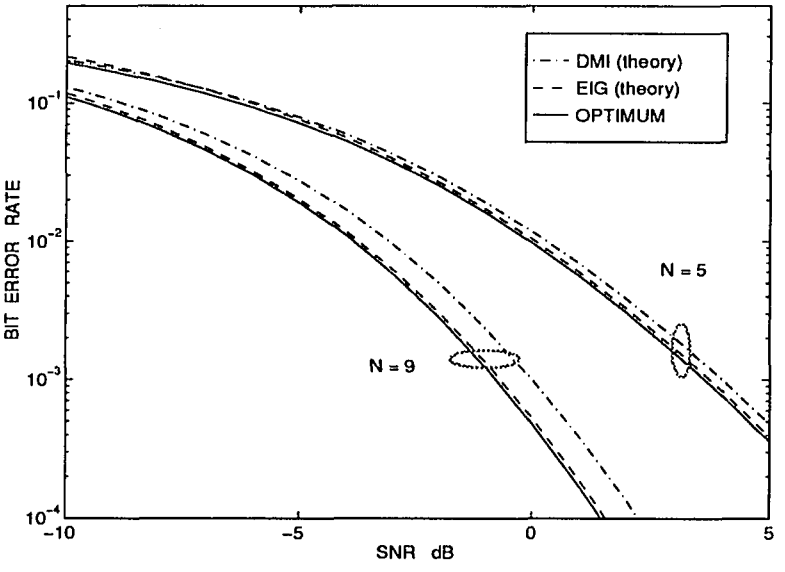

(b) K=50

Figure 2.3 The average BER vs. the average received SNR with one interference when INR=2 dB and (a) K=20, (b) K=50 (analytical results)

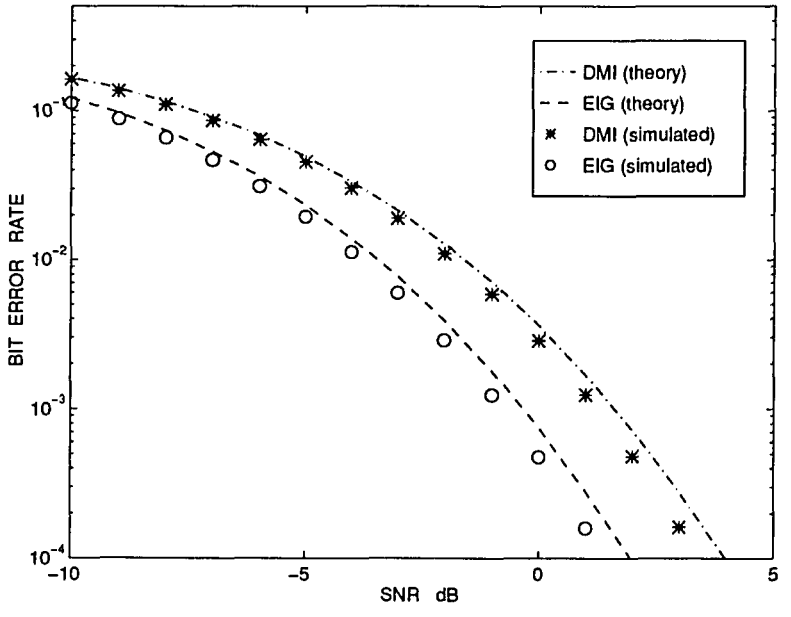

Figure 2.4 The average BER vs. the average received SNR with one interference, N=9 and K=20 (simulation results)

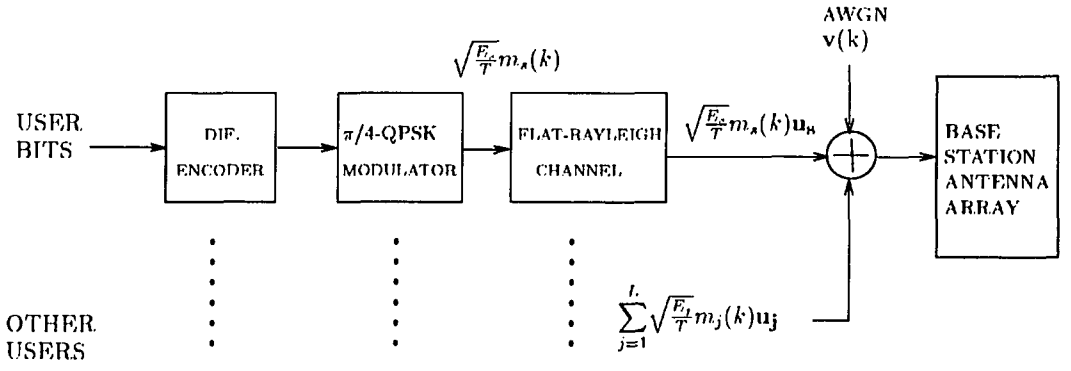

Figure 2.5 IS-54 data model

2.5 Application of IS-54

The proposed IS-54 TDMA system uses $\pi/4$-shifted DQPSK modulation which maps a 2-bit symbol to the differential phase $\Delta\phi(k) = \phi(k) - \phi(k-1)$, where $\phi(k)$ is the kth phase of the carrier and $\Delta\phi(k) = (2m-3)\pi/4$ with $m = 0, 1, 2, 3$. The transmitted data symbol is presented as $m(k) = \exp(j\phi(k))$. The probability of error for $\pi/4$-DQPSK is given by [1]:

$$P_e(\gamma) = \frac{1}{4\pi\sqrt{2}} \int_0^{2\pi} \frac{1}{1 - \frac{\cos t}{\sqrt{2}}} \exp\left[-\gamma\left(1 - \frac{\cos t}{\sqrt{2}}\right)\right] dt. \tag{2.28}$$

A typical IS-54 TDMA frame contains three time slots. Each slot contains 324 bits consisting of a 28-bit synchronization sequence, a 12-bit user identification sequence and a 260-bit data sequence. Only a 14 DQPSK symbol (28 bits) synchronization sequence is used as training sequence, i.e., $K = 14$. The energy per bit to noise power density ratio for DQPSK is given by:

$$\frac{E_b}{N_o} = \frac{E_s}{N_o}\frac{1}{2}. \tag{2.29}$$

Where E_s is the symbol energy. The carrier-to-interference ratio (CIR) at each element is defined as:

$$\mathrm{CIR} = \frac{\mathrm{SNR}}{\mathrm{INR}}, \tag{2.30}$$

where SNR and INR are defined in eqs. (2.26) and (2.27), respectively.

In Figure 2.6, the CIR is equal to 1.8 dB. This figure presents the average BER versus the received E_b/N_o for N=9 and N=12, respectively, for one interference case. Both analytical results and simulation results indicate that, when the number of antenna increases from 9 to 12, the DMI method fails to further improve the system performance. However, the eigencanceler improves the system performance.

For the case of multiple interferences only simulation results are presented. With all channels fully occupied, we consider 6 co-channel interferences from the first layer, 12 from the second layer and 18 from the third layer while ignoring interferences from layers further away as shown in Figure 2.7. The power of the interference of the first layer is proportional to r^{-4}, where r is distance from the interference mobile to cell site. The power of the interference of the second and third layers is assumed to be proportional to r^{-7} [28]. The normalized eigenvalue distribution of the interference and noise covariance matrix of this model is shown in Figure 2.8. Most of the interferences power concentrated in the 6 largest eigenvalues, the eigencanceler can still be applied and can perform superior to the DMI method, provided that the number of antennas is large enough. For a given frequency reuse pattern, the system provides a certain level of CIR. The relation between CIR and the frequency reuse factor can be found in ref. [3]:

$$\left(\frac{C}{I}\right)_{\mathrm{ave}} = \frac{1}{6q^{-4}} \tag{2.31}$$

where q is the cochannel interference reduction factor defined as $q = \sqrt{3F}$. F is the frequency reuse factor. In a real case scenario, the CIR can be 4 dB or 8 dB worse than the specified value. Table 2.1 summarizes this relation [36].

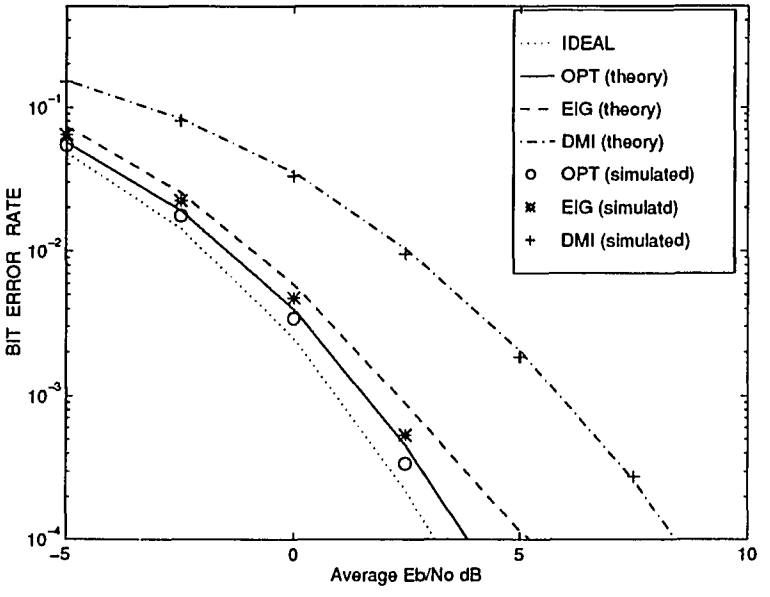

(a) N=9

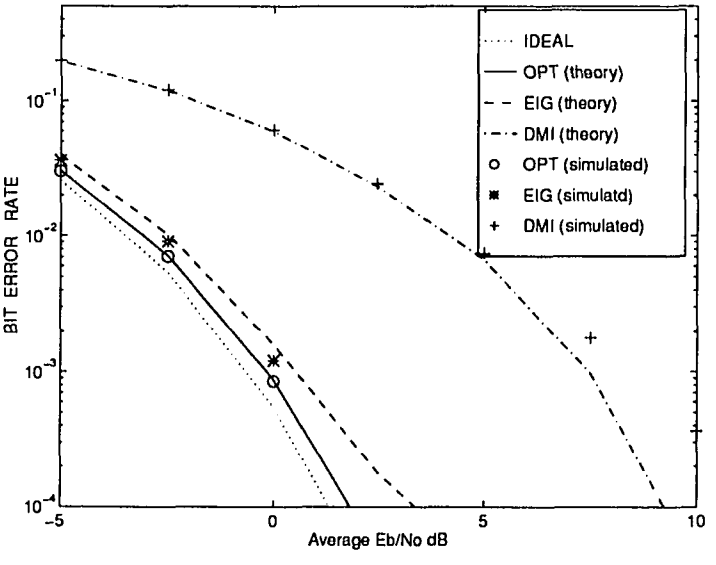

(b) N=12

Figure 2.6 The average BER vs. the received E_b/N_o with one interference when CIR=1.8 dB and (a) N=9, (b) N=12

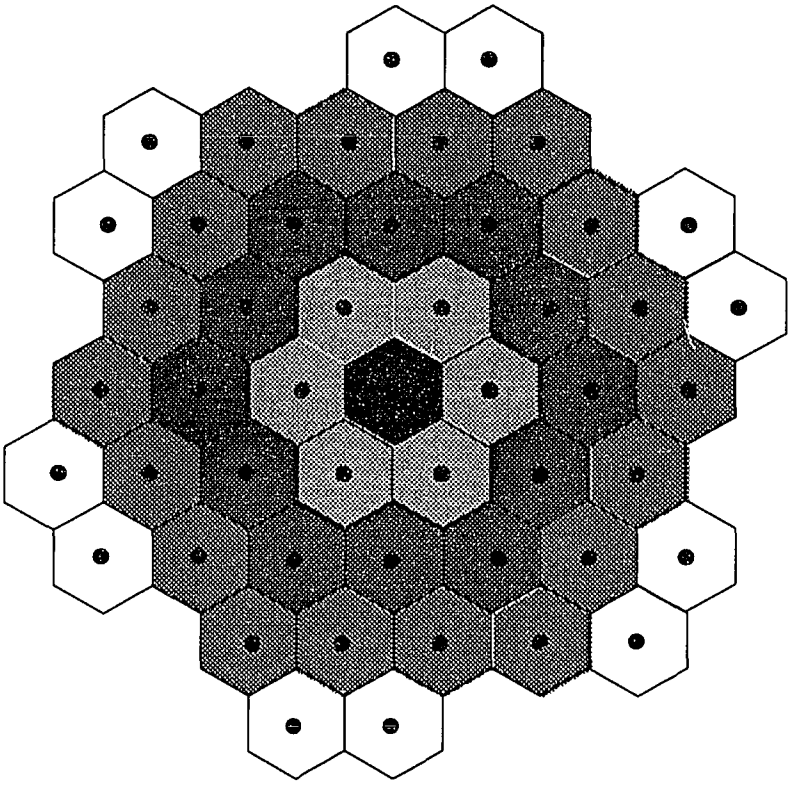

Figure 2.7 Cell layers

Reuse Factor	CIR (dB) (average)	CIR (dB) (worst)
1	1.8	-7.8
3	11.3	4.3
4	13.8	7.9
7	18.7	14.4

Table 2.1 Frequency reuse factor and CIR

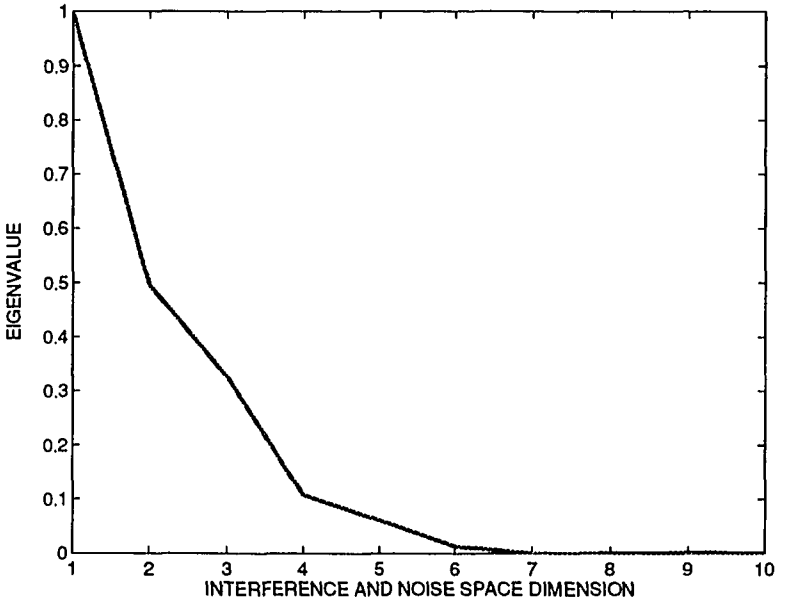

Figure 2.8 Eigenvalue distribution of received interference plus noise covariance matrix

Let us consider N=12 antennas. Figure 2.9 shows the average BER versus the average received E_b/N_o with CIR =1.8 dB which implies a frequency reuse factor of 1 for the average case. Figure 2.9 indicates that the eigencanceler requires 5 dB less of signal power for a BER of 10^{-3} than the DMI method.

Figure 2.10 shows the average BER versus the average received CIR for an adaptive array with given signal power. Figure 2.10 (a) shows an ideal case, i.e., low noise power situation $N_o \rightarrow 0$, where the system capacity is restricted only by the cochannel interferences. The eigencanceler reduces CIR requirements by 1 dB as compared with DMI method. Figure 2.10 (b) shows that when E_b/N_o= 10 dB, the DMI requires 10 dB CIR level while the eigencanceler requires only -5 dB. The latter can almost satisfy the CIR requirement for the worst case CIR for reuse factor of 1 as per Table 2.1.

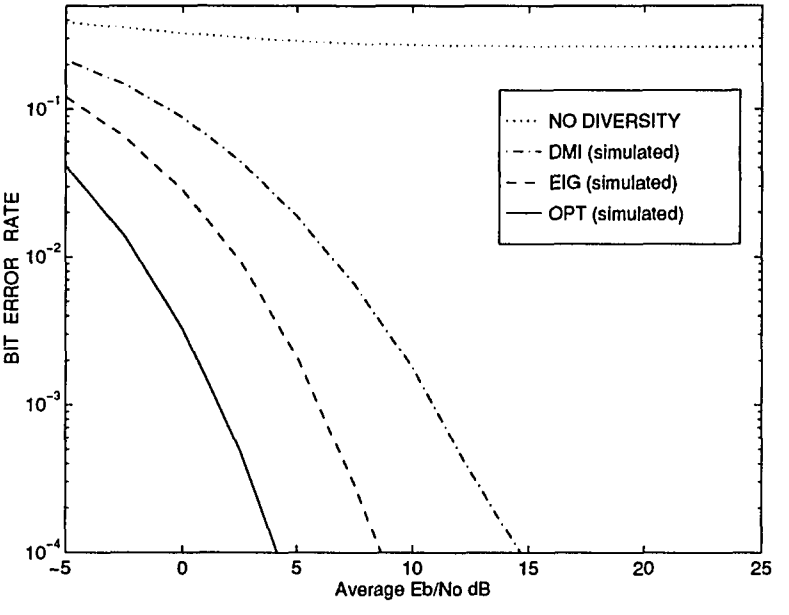

Figure 2.9 The average BER vs. the average received E_b/N_o for an adaptive array with CIR=1.8 dB (simulation results)

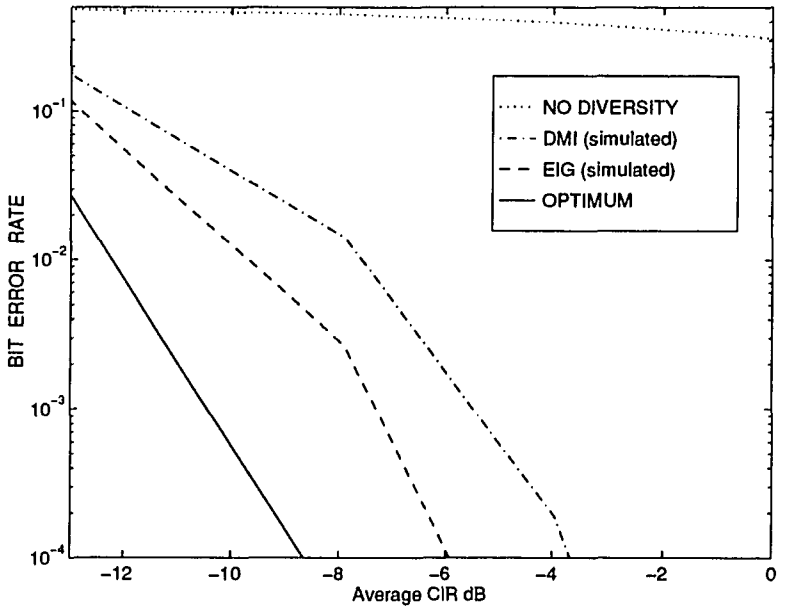

(a) E_b/N_o = 100 dB

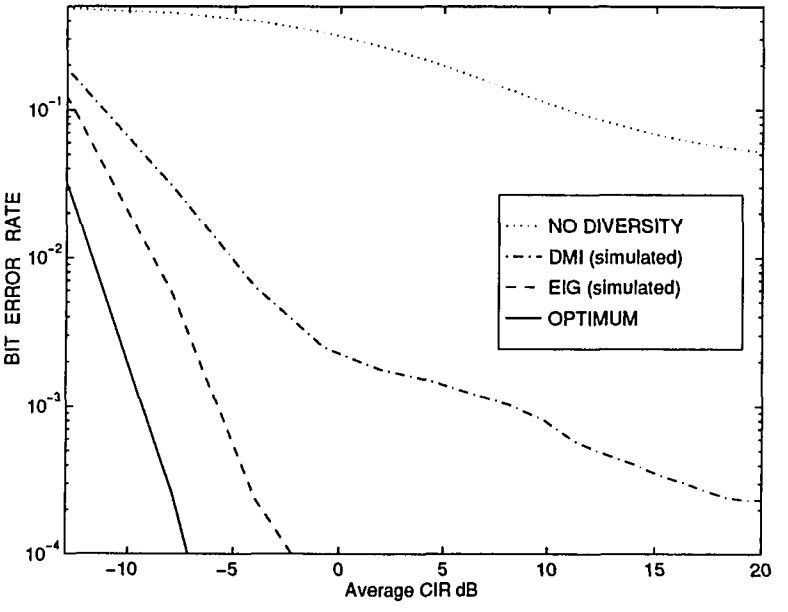

(b) E_b/N_o = 10 dB

Figure 2.10 The average BER vs. the CIR when N=12 and (a) E_b/N_o=100 dB, (b) E_b/N_o=10 dB

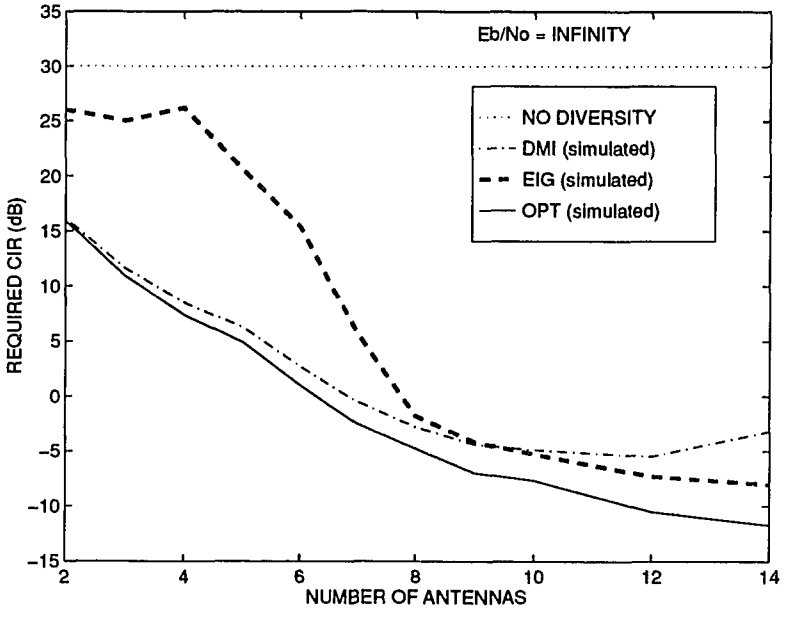

(a) E_b/N_o = 100 dB

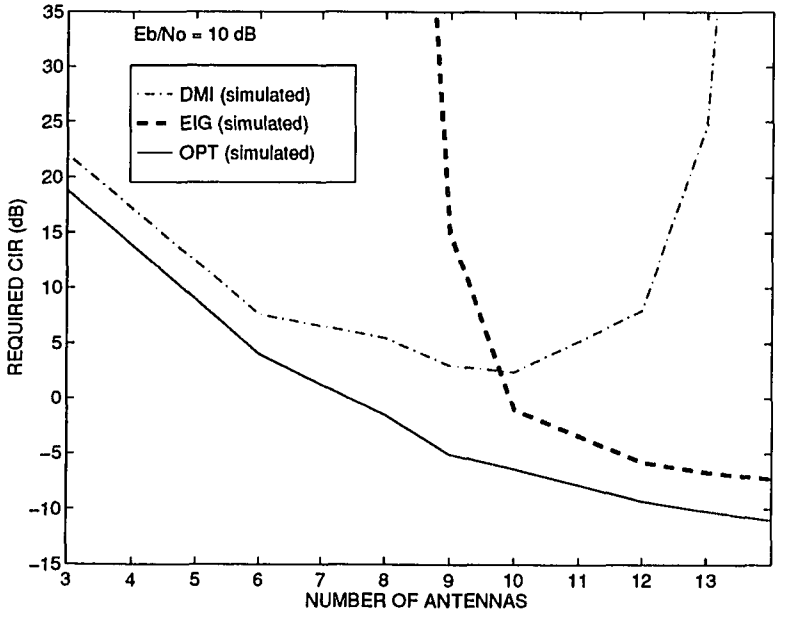

(b) E_b/N_o = 10 dB

Figure 2.11 The required CIR vs. the number of antennas at BER $=10^{-3}$ when (a) E_b/N_o=100 dB, (b) E_b/N_o=10 dB

Figure 2.11 shows the CIR requirement versus the number of the antennas at a BER of 10^{-3}. With $N_o \rightarrow 0$, Figure 2.11 (a) shows that the eigencanceler can achieve superior performance over the DMI method when the number of antennas is larger than 10. When E_b/N_o= 10 dB, Figure 2.11 (b) shows that the eigencanceler can reduce the CIR requirement below 0 dB while the DMI method can not.

2.6 Summary

Adaptive spatial processing to increase TDMA system capacity has been studied. The estimation of an array covariance matrix entails a loss in the array output SNIR with respect to the optimal case of a known covariance matrix. The density function of this loss has been derived elsewhere for both the DMI and the eigenanalysis-based methods and is used to develop an analytical expression for the average probability of error for each method for single interference. It is shown that the eigenanalysis-based method has performance close to the optimal in some cases and is superior to the performance of the DMI method. Simulations are used to corroborate the analytical results.

CHAPTER 3

IMPLEMENTATION

In Chapter 2, we presented spatial processing techniques mainly for block processing. Block processing for both *optimum combining* and the *eigencanceler* require $O(N^3)$ flops per data block. Adaptive algorithms provide continuous tracking and have lower computational requirements. LMS and RLS are two common algorithms used to implement optimum combining. In this chapter, we demonstrate our new projection-based method [37] and the power method to implement the eigencanceler, and compare their performance with the LMS and RLS algorithms.

3.1 Adaptive Algorithms for the Eigencanceler

The eigencanceler requires decomposition of the signal space into interference/noise subspaces. Traditionally this has been achieved using either *eigenvalue decomposition* (EVD) or *singular value decomposition.* The full decompositions, however, are computationally inefficient, requiring $O(N^3)$ flops and hence they are not suited for real-time data applications. In recent years new adaptive algorithms have been suggested for subspace tracking [29, 25]. Next, we suggest a new, simple algorithm for updating the interference subspace and the eigencanceler's weight vector.

3.1.1 Projection Algorithm

Let r be the rank of the interference subspace. Then, the algorithm consists of the following steps.

1. Initialize the interference subspace, for example $\widehat{\mathbf{Q}}_c(0) = \mathbf{I}_r$, and initialize $\hat{\mathbf{r}}_{sx}(0)$. $\mathbf{I}_r$ is a N by r matrix defined as

$$\mathbf{I}_r = \begin{bmatrix} 1 & \dots & 0 \\ \vdots & \ddots & \vdots \\ 0 & \dots & 1 \\ 0 & \dots & 0 \\ \vdots & \ddots & \vdots \\ 0 & \dots & 0 \end{bmatrix}. \tag{3.1}$$

2. Update the interference subspace using the new interference-plus-noise data at time k:

$$\widetilde{\mathbf{Q}}_c(k) = \left(\mathbf{I} + \mu \frac{\tilde{\mathbf{x}}(k)\tilde{\mathbf{x}}^H(k)}{\|\tilde{\mathbf{x}}(k)\|^2}\right) \widehat{\mathbf{Q}}_c(k-1), \tag{3.2}$$

where μ is a forgetting factor and $\tilde{\mathbf{x}}(k)$ is the estimate interference-plus-noise vector.

3. Orthogonalize the columns of $\widetilde{\mathbf{Q}}_c(k)$ using the Gram-Schmidt procedure:

$$\widehat{\mathbf{Q}}_c(k) = \text{orth}\left[\widetilde{\mathbf{Q}}_c(k)\right]. \tag{3.3}$$

4. Update the cross-correlation vector:

$$\hat{\mathbf{r}}_{sx}(k) = \gamma \hat{\mathbf{r}}_{sx}(k-1) + m_s^*(k)\tilde{\mathbf{x}}(k), \tag{3.4}$$

where γ is a forgetting factor and $m_s(k)$ is a data symbol the SOI.

5. Update the array weight vector:

$$\mathbf{w}(k) = \left[\mathbf{I}_r - \widehat{\mathbf{Q}}_c(k)\,\widehat{\mathbf{Q}}_c^H(k)\right] \hat{\mathbf{r}}_{sx}(k). \tag{3.5}$$

The algorithm involves tracking the interference subspace and the cross-correlation vector, followed by updating the weight vector. The first step updates the interference subspace using the received interference-plus-noise data $\tilde{\mathbf{x}}(k)$. The resulting matrix $\widetilde{\mathbf{Q}}_c(k)$ does not necessarily have orthogonal columns. Those columns are orthogonalized in Step 3.

3.1.2 Power Method

A more complex algorithm for updating the interference subspace and the eigen-canceler's weight vector is a power method:

1. Initialize the correlation matrix $\hat{\mathbf{R}}_n(0) = \mathbf{I}$, cross-correlation vector $\hat{\mathbf{r}}_{sx}(0) = \zeta\mathbf{1}$, and the interference subspace $\hat{\mathbf{Q}}_c(0) = \mathbf{I}_r$, where $\mathbf{I}$ is the N by N identity matrix, $\mathbf{1} = [1, 1, \ldots, 1]^T$, and ζ is a small number.

2. Update the correlation matrix using the new interference-plus-noise data at time k:

$$\hat{\mathbf{R}}_n(k) = \mu_p \hat{\mathbf{R}}_n(k-1) + \frac{\tilde{\mathbf{x}}(k)\tilde{\mathbf{x}}^H(k)}{\|\tilde{\mathbf{x}}(k)\|^2}. \tag{3.6}$$

3. Update the interference subspace based on the correlation matrix:

$$\widetilde{\mathbf{Q}}_c(k) = \hat{\mathbf{R}}_n(k)\,\hat{\mathbf{Q}}_c(k-1). \tag{3.7}$$

4. Follow steps 3, 4 and 5 in the projection-based algorithm by using eqs. (3.3)(3.4) and (3.5).

The adaptive algorithms require the use of a reference signal (denoted $r(k)$ in eq. (3.4) above) correlated with the SOI and uncorrelated with the interferences. The reference signal may be generated with a number of techniques. For example, the reference could be initially supplied by a training sequence and then derived from direct symbol detection at the array output. The quality of this detection is obviously unsatisfactory for communication, but if the interference is not too strong, it may be sufficient for supplying the reference. Alternatively, the reference could be derived by using spread spectrum techniques, as suggested in [2]. The interference plus noise vector $\tilde{\mathbf{x}}(k)$ may be computed, noting that $r(k)\,\hat{\mathbf{r}}_{sx}(k)$ provides an estimate of the SOI,

$$\tilde{\mathbf{x}}(k) = \mathbf{x}(k) - m_s(k)\,\hat{\mathbf{r}}_{sx}(k). \tag{3.8}$$

The computational complexity of the projection algorithm is $O(Nr^2)$ and is determined by the Gram-Schmidt orthogonalization. This complexity is more than the $O(N)$ complexity of the LMS algorithm and, for $r \leq \sqrt{N}$, it is less than the $O(N^2)$ complexity of the RLS. Thus, the new algorithm is particularly suited to cases with a low-rank interference subspace. The complexity of the power method is $O(N^3)$.

3.2 Derivation of the Projection Algorithm

The previous section proposed two adaptive algorithms for the eigencanceler. The convergence of power method is proven in [7]. In this section, we will derive the projection-based algorithm.

First, Let us consider one interference case. Assuming vector $\mathbf{q}_1$ is the eigenvector of $\mathbf{R}_n$ corresponding to the largest eigenvalue λ_1, we have $\lambda_1 \mathbf{q}_1 = \mathbf{R}_n \mathbf{q}_1$. Based on this equation, we can build an adaptive scheme as follows:

$$\begin{aligned} \lambda_1 \mathbf{q}_1(k) &= \mathbf{R}_n(k)\mathbf{q}_1(k-1) \\ &= \left[\mathbf{R}_n(k-1) + \mu \frac{\tilde{\mathbf{x}}(k)\tilde{\mathbf{x}}^H(k)}{\|\tilde{\mathbf{x}}(k)\|^2}\right] \mathbf{q}_1(k-1) \\ &= \lambda_1 \mathbf{q}_1(k-1) + \mu \frac{\tilde{\mathbf{x}}(k)\tilde{\mathbf{x}}^H(k)}{\|\tilde{\mathbf{x}}(k)\|^2} \mathbf{q}_1(k-1). \end{aligned} \tag{3.9}$$

Dividing both sides by λ_1, we have the interference subspace updating equation:

$$\mathbf{q}_1(k) = \left(\mathbf{I} + \frac{\mu}{\lambda_1} \frac{\tilde{\mathbf{x}}(k)\tilde{\mathbf{x}}^H(k)}{\|\tilde{\mathbf{x}}(k)\|^2}\right) \mathbf{q}_1(k), \tag{3.10}$$

which is equivalent to the projection method for the one interference case.

Next, Let us consider a two-interference case. Following the same idea, we extend eq. (3.10) to a two-column matrix format as follows:

$$[\bar{\mathbf{q}}_1(k) \quad \bar{\mathbf{q}}_2(k)] = [\mathbf{q}_1(k-1) \quad \mathbf{q}_2(k-1)] + \mu \frac{\tilde{\mathbf{x}}(k)\tilde{\mathbf{x}}^H(k)}{\|\tilde{\mathbf{x}}(k)\|^2} \left[\frac{1}{\lambda_1}\mathbf{q}_1(k-1) \quad \frac{1}{\lambda_2}\mathbf{q}_2(k-1)\right] \tag{3.11}$$

$$[\mathbf{q}_1(k) \quad \mathbf{q}_2(k)] = \text{orth}\,[\bar{\mathbf{q}}_1(k) \quad \bar{\mathbf{q}}_2(k)]. \tag{3.12}$$

The resulting matrix in eq. (3.11) does not necessarily have orthogonal columns. Those columns are orthogonalized in eq. (3.12). This adaptive scheme requires the estimation of the eigenvalues. After simplifying eq. (3.11), we get so-called the projection-based algorithm:

$$[\tilde{\mathbf{q}}_1(k) \quad \tilde{\mathbf{q}}_2(k)] = \left[\mathbf{I} + \mu \frac{\tilde{\mathbf{x}}(k)\tilde{\mathbf{x}}^H(k)}{\|\tilde{\mathbf{x}}(k)\|^2}\right] [\hat{\mathbf{q}}_1(k-1) \quad \hat{\mathbf{q}}_2(k-1)] \tag{3.13}$$

$$[\hat{\mathbf{q}}_1(k) \quad \hat{\mathbf{q}}_2(k)] = [\tilde{\mathbf{q}}_1(k) \quad \tilde{\mathbf{q}}_2(k)]. \tag{3.14}$$

This projection method avoids estimating the eigenvalues. Next, we will show that the method is equivalent to the adaptive method represented by eqs. (3.11) and (3.12). Our goal is to show that span $[\mathbf{q}_1(k) \quad \mathbf{q}_2(k)]$ equals span $[\hat{\mathbf{q}}_1(k) \quad \hat{\mathbf{q}}_2(k)]$. We will use induction method to prove this. Let us assume that:

$$\text{span}\,[\mathbf{q}_1(k-1) \quad \mathbf{q}_2(k-1)] = \text{span}\,[\hat{\mathbf{q}}_1(k-1) \quad \hat{\mathbf{q}}_2(k-1)]. \tag{3.15}$$

From eqs. (3.11) and (3.12), we have:

$$\begin{aligned} \text{span}\,[\mathbf{q}_1(k) \quad \mathbf{q}_2(k)] &= \text{span}\,[\bar{\mathbf{q}}_1(k) \quad \bar{\mathbf{q}}_2(k)] \\ &= \text{span}\,[\mathbf{q}_1(k-1) \quad \mathbf{q}_2(k-1)]. \\ &\quad + \text{span}\left\{\mu \frac{\tilde{\mathbf{x}}(k)\tilde{\mathbf{x}}^H(k)}{\|\tilde{\mathbf{x}}(k)\|^2} \left[\frac{1}{\lambda_1}\mathbf{q}_1(k-1) \quad \frac{1}{\lambda_2}\mathbf{q}_2(k-1)\right]\right\} \\ &= \text{span}\,[\mathbf{q}_1(k-1) \quad \mathbf{q}_2(k-1)] \\ &\quad + \text{span}\left\{\mu \frac{\tilde{\mathbf{x}}(k)\tilde{\mathbf{x}}^H(k)}{\|\tilde{\mathbf{x}}(k)\|^2} [\mathbf{q}_1(k-1) \quad \mathbf{q}_2(k-1)]\right\}. \end{aligned} \tag{3.16}$$

From eqs. (3.13) and (3.14), we have:

$$\begin{aligned}\text{span}\,[\hat{\mathbf{q}}_1(k) \quad \hat{\mathbf{q}}_2(k)] &= \text{span}\,[\tilde{\mathbf{q}}_1(k) \quad \tilde{\mathbf{q}}_2(k)]\,. \\ &= \text{span}\,[\hat{\mathbf{q}}_1(k-1) \quad \hat{\mathbf{q}}_2(k-1)] \\ &\quad +\text{span}\left\{\mu\frac{\tilde{\mathbf{x}}(k)\tilde{\mathbf{x}}^H(k)}{\|\tilde{\mathbf{x}}(k)\|^2}\,[\hat{\mathbf{q}}_1(k-1) \quad \hat{\mathbf{q}}_2(k-1)]\right\}. \quad (3.17)\end{aligned}$$

With the assumption of eq. (3.15), the righthand sides of eqs. (3.16) and (3.17) are equal. Thus, we can conclude that the two adaptive schemes are equivalent.

The algorithm requires knowledge of the rank of the interference subspace. An additional step may be incorporated in the algorithm to estimate and track changes in the rank of the interference subspace. To that end, note that the interference eigenvalues are given by

$$\mathrm{E}\left[\widehat{\mathbf{Q}}_c(k-1)\tilde{\mathbf{x}}(k)\tilde{\mathbf{x}}^H(k)\widehat{\mathbf{Q}}_c(k-1)\right] = \mathbf{\Lambda}_c. \quad (3.18)$$

Thus $\widehat{\mathbf{Q}}_c^H(k-1)\tilde{\mathbf{x}}(k)\tilde{\mathbf{x}}^H(k)\widehat{\mathbf{Q}}_c(k-1)$ provides an estimate of the interference eigenvalues at each update. The rank of the interference subspace may be adjusted based on significant changes in the size of the smallest eigenvalue of the interference subspace.

3.3 Results

The projection-based algorithm and the power method were evaluated with simulations and compared to the LMS and RLS algorithms. The reference signals were estimated using an 8-chip long, pseudo-noise sequence. Propagation vector components were modeled as i.i.d. complex Gaussian random variables. Propagation vectors were assumed to be constant over processing time. The simulations were carried out for $M = 9$ elements, SNR = 2 dB, and INR = 2 dB. The results presented below were obtained by averaging 400 independent runs. Figure 3.1(a) shows the learning curve of the BER for a single interference and Figure 3.1(b) presents the

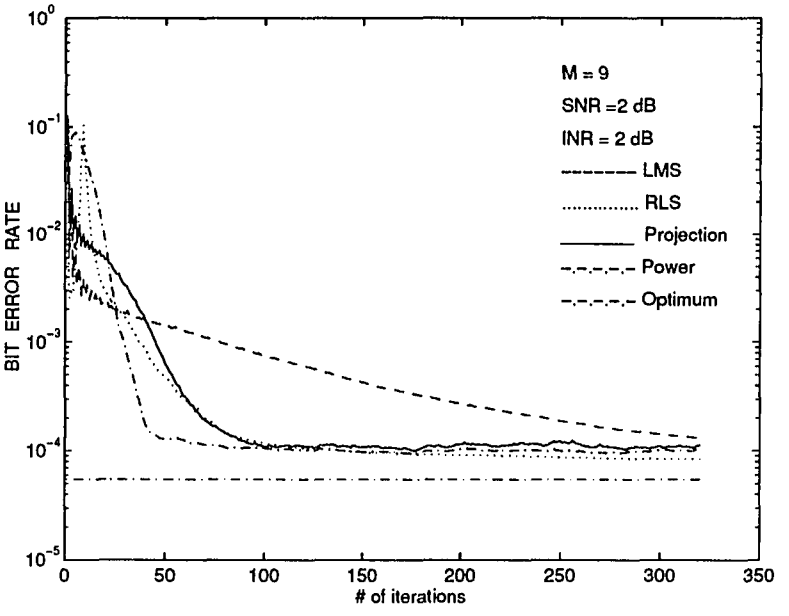

(a) One interference

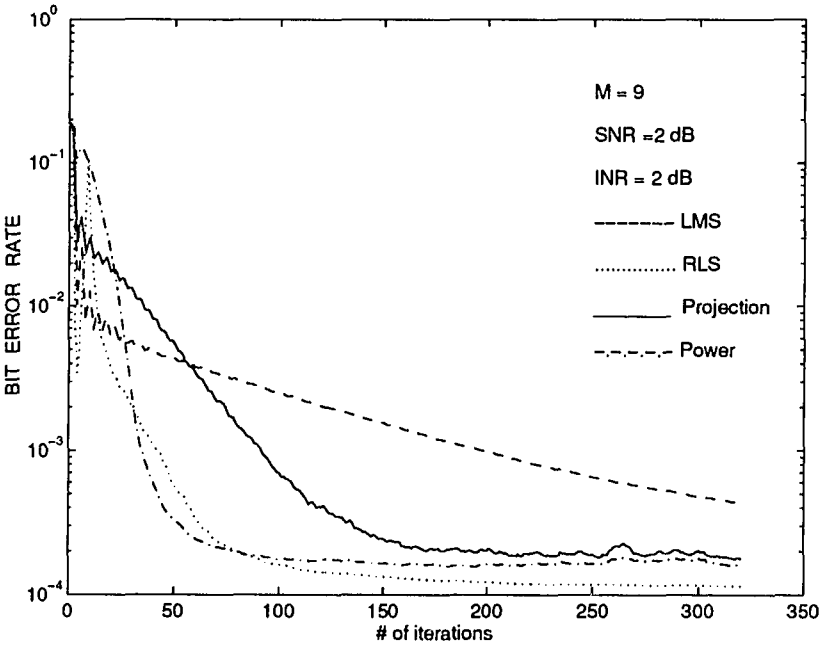

(b) Two interferences

Figure 3.1 The average BER vs. the number of iterations with (a) one interference, (b) two interferences

case for two interferences. The BER at each run was calculated assuming a Gaussian distribution of the interference-plus-noise at the array output

$$P(e \mid \mathbf{u}_s, \mathbf{u}_j) = Q\left(\frac{\mathbf{w}^H \mathrm{E}\left[\mathbf{x}_s(k)\mathbf{x}_s^H(k) \mid \mathbf{u}_s\right]\mathbf{w}}{\mathbf{w}^H \mathrm{E}\left[\tilde{\mathbf{x}}(k)\tilde{\mathbf{x}}^H(k) \mid \mathbf{u}_j\right]\mathbf{w}}\right), \tag{3.19}$$

where $Q(\cdot) = 0.5\,\mathrm{erfc}(\cdot/\sqrt{2})$. The plot shows the BER averaged over 100 independent the propagation vectors. In addition, we have included a line representing the value of the BER for optimum combining at steady state for the case of one interference, and calculated using eq. (25) in [33]. For one interference the new algorithm's speed is comparable to the RLS. For two interferences the projection-based algorithm is faster than the LMS and slower than the RLS.

Furthermore, let us consider a dynamic system. The fading environment is changed predominantly by the movement of mobiles. We use an AR process to model the slow fading:

$$\mathbf{u}(k) = \xi\mathbf{u}(k-1) + \eta(k) \quad \text{where} \quad 0 < \xi \leq 1,\ k = 1, 2, 3, \ldots \tag{3.20}$$

with the constraints $E[|u_i(k)|^2 \mid u_i(0)] = |u_i(0)|^2$, $i = 1, \ldots, N$ to maintain equal power of process samples. The variance of white Gaussian noise $\eta(k)$ is: $E[|\eta_i(k)|^2] = (1-\xi^2)|u_i(0)|^2$.

This 3 dB bandwidth ω_p of this AR process is determined by the speed of the mobile v, and can be written as follows:

$$\omega_p = \frac{2\pi v T}{\lambda}, \tag{3.21}$$

where λ is the wavelength and T is the symbol interval. The amplitude response $|H(e^{j\omega})|$ of this AR process is as follow:

$$|H(e^{j\omega})| = \frac{1}{(1+\xi^2-2\xi\cos\omega)^{1/2}}. \tag{3.22}$$

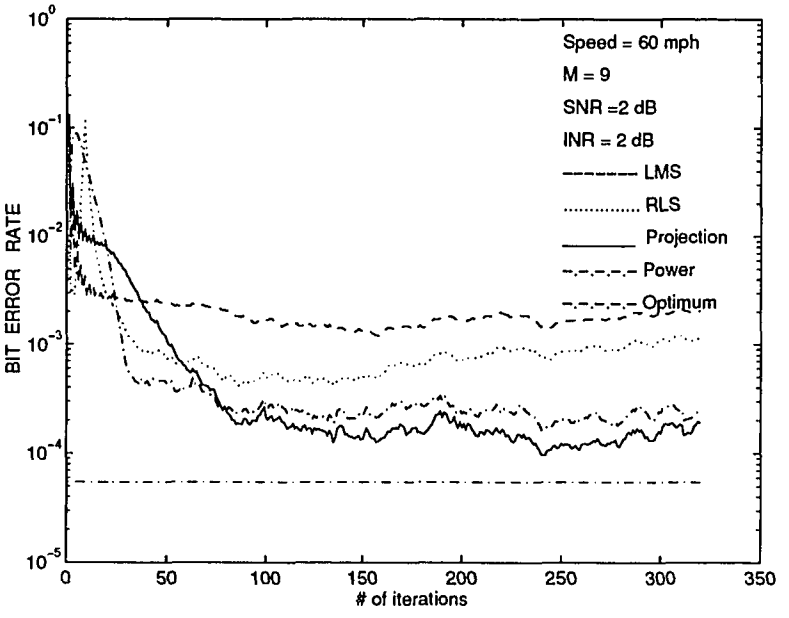

Figure 3.2 Tracking ability

Let $|H(e^{j0})|/|H(e^{j\omega_p})| = 2$, we have the relation between ξ and ω_p:

$$\xi = \frac{-b - \sqrt{b^2 - 4}}{2} \quad \text{where} \quad b = \frac{-8 + 2\cos(\omega_p)}{3}. \tag{3.23}$$

Figure 3.2 presents simulation results of the system tracking ability with a mobile travelling at 60 mph or about 100 km/h. It shows that the projection-based method has the best performance in terms of tracking SOI.

CHAPTER 4

SPACE-TIME PROCESSING FOR CDMA COMMUNICATIONS

As discussed earlier, spatial processing can be used to improve the performance and capacity of narrow-band TDMA systems. Next, we extend this technique to combined spatial-temporal processing [39] to improve wide-band CDMA system performance and capacity.

A SMRC/TMRC system could exploit the diversity in both the spatial and temporal domains. MRC in the temporal domain is also the concept underlying the RAKE receiver. The MRC method is optimal when the noise is white; however, it does not eliminate co-channel interference. Hence, a different approach is needed to overcome *near-far effects.* A solution to this problem is offered by adaptive antennas. In contrast to MRC, *optimum combining* refers to the maximization of the SNIR. The application of optimum combining rather than MRC is motivated by the observation that the co-channel interference is colored, as illustrated in the eigenvalues distribution of the example in Figure 4.1. In this chapter, the applications of various space-time processing schemes, such as SMRC/TMRC, SOPT/TMRC, SOPT/TOPT and JOPT schemes, are studied for the CDMA-based wireless communication systems.

The chapter is organized as follows: Section 4.1 contains the signal model, in Section 4.2 we formulate the processing schemes and derive the associated space-time filters weights, numerical results are given in Section 4.3, and the conclusions are summarized in section 4.5

4.1 Signal Model

Consider a cell site that serves $L+1$ users. The signal transmitted by the designated user is denoted $g_0(t)$, while signals transmitted by the other users are denoted $g_j(t)$, $j = 1, \ldots, L$. The signals $g_j(t)$ are considered co-channel interference with

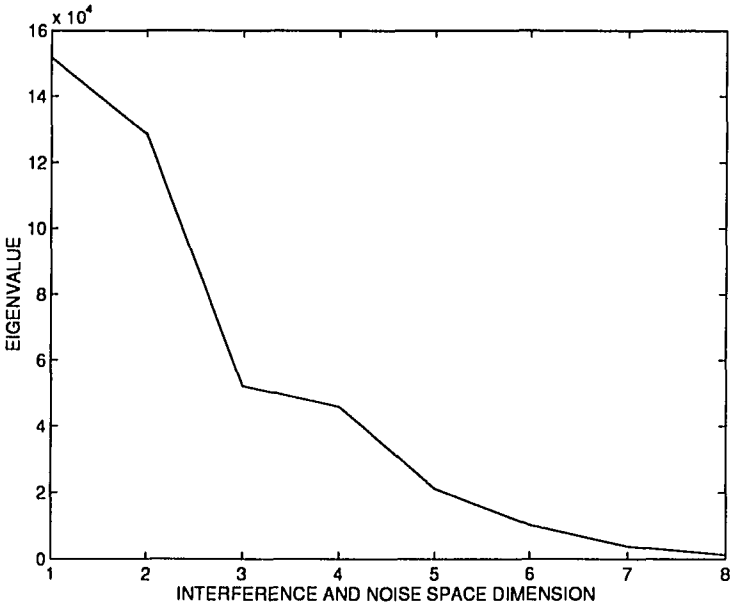

Figure 4.1 Eigenvalues of the space-time covariance matrix for N=2 antennas, M=4 taps, and L=70 users.

respect to the designated user. The equivalent lowpass transmitted waveform for the ith user is

$$g_i(t) = A_i\, S_i\left(\lfloor \frac{t}{T_s} \rfloor\right) u_i(t), \tag{4.1}$$

where A_i denotes the amplitude of the signal. The amplitude of the signal transmitted by co-channel interference user j is $A_j = \psi_j\sqrt{P_j}$, where P_j is the power and ψ_j represents the voice activity modeled as a constant 3/8 for $j = 1, \ldots, L$. In the case of perfect power control, all P_j's are equal. Imperfect power control is characterized by the *power control error* (PCE) parameter. The notation ($\lfloor \cdot \rfloor$) denotes the integer part, and $S_i(t)$ is the binary information data bit transmitted by the ith user with $E[|S_i(t)|^2] = 1$. The users' signature waveforms, i.e., spreading waveforms, are represented by time functions $u_i(t)$, with period T_s, where T_s is the

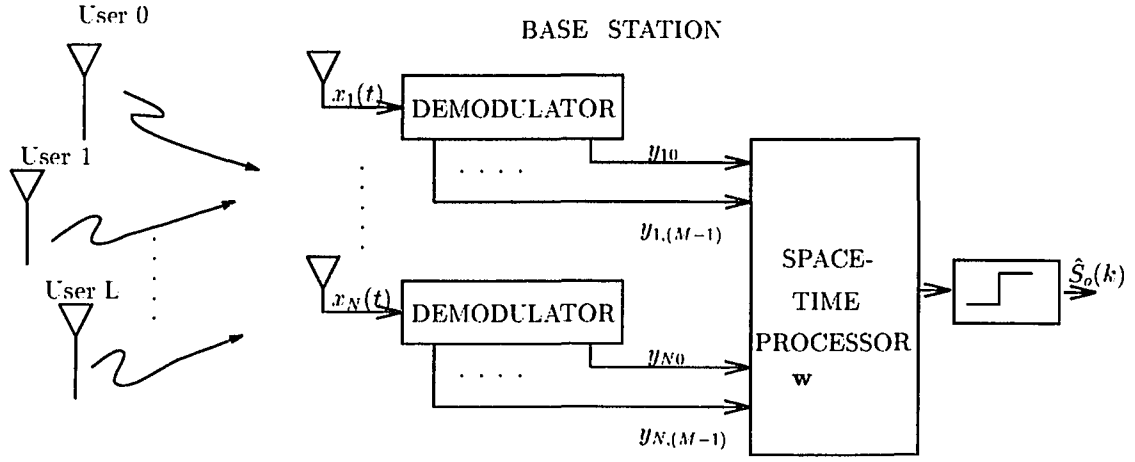

Figure 4.2 General configuration of the space-time CDMA receiver

symbol interval. The spreading gain is given by $D = T_s/T_c$, with unit chip duration $T_c = 1$, $D = \int_0^{T_s} |u_i(t)|^2 dt$.

The typical CDMA channel is frequency-selective, i.e., the channel coherence bandwidth Δf_c is assumed smaller than the transmitted signal bandwidth W. This channel coherence bandwith is determined by the multipath spread T_m, with $\Delta f_c = 1/T_m$. Such a channel can be modeled with M resolvable paths [24], where $M = [T_m W] + 1$. It is assumed that $T_s > T_m$.

The general configuration at the base station is shown in Figure 4.2. The base station uses an N-element uniform array with antennas set sufficiently apart such that the signals can be assumed to reach the antennas via independent paths, and hence can be modeled as independent random processes. We further assume perfect code synchronization. The signal received at nth antenna can be written:

$$\begin{aligned} x_n(t) &= \sum_{m=0}^{M-1} C_{nm}^{(0)}(t)\, g_0(t - mT_d - \tau_0) \\ &\quad + \sum_{j=1}^{L} \sum_{m=0}^{M-1} C_{nm}^{(j)}(t)\, g_j(t - mT_d - \tau_j) + v_n(t) \end{aligned} \tag{4.2}$$

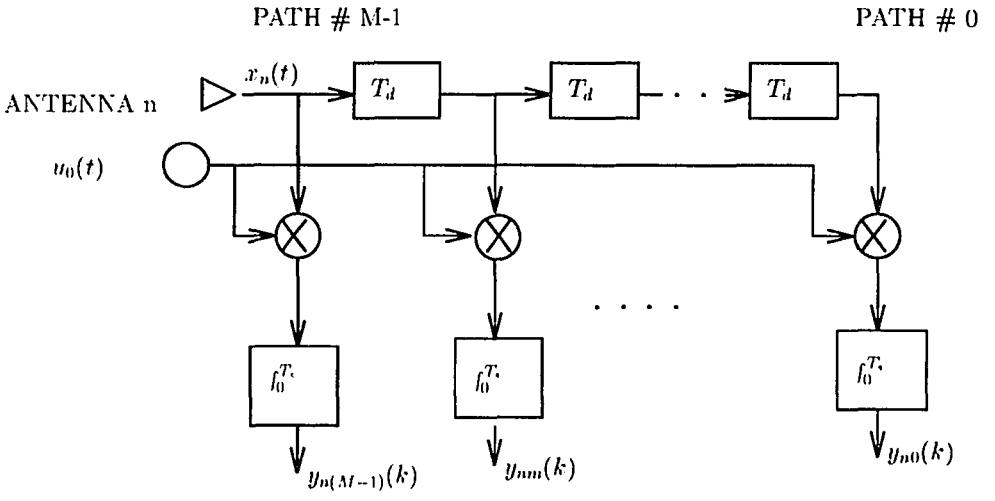

Figure 4.3 Configuration of the demodulator

where $C_{nm}^{(j)}(t)$, $j = 0, \ldots, L$, $m = 0, \ldots, M-1$ are random processes characterizing the fading channel as seen by each of the users. Samples of $C_{nm}^{(j)}(t)$ are modeled as zero-mean, complex-valued, stationary Gaussian random processes—statistically independent between users j and between paths m. The received signals are assumed asynchronous, with τ_j denoting the delay of the jth user with respect to an arbitrary time origin. $T_d = 1/W$ represents the tap-delay in the channel model. The additive noise $v_n(t)$ is modeled white complex Gaussian with a variance of σ_v^2. We further assume that the channel is characterized by slow fading such that $C_{nm}^{(j)}(t) = C_{nm}^{(j)}$ during the processing period. Without loss of generality we set the time origin such that $\tau_0 = 0$.

A demodulator is used at each antenna element to collect the energy of the received signal from all the independent paths and despread signals. The demodulator consists of an M-tap delay line and matched filters. The tap-delay line compensates for the delay propagation in the channel, providing the time alignment for demodulation with the user's signature $u_0(t)$. The received signal at the nth

antenna passes through the tap delay line and is fed into the correlators for spread spectrum demodulation. The output at the mth tap correlator and the kth symbol is given by:

$$\begin{aligned} y_{nm}(k) &= \int_{kT_s}^{(k+1)T_s} x_n(t+mT_d)u_0^*(t)dt \\ &= \int_{kT_s}^{(k+1)T_s} \sum_{i=0}^{M-1} C_{ni}^{(0)}\, g_0(t+mT_d-iT_d)u_0^*(t)\,dt \\ &\quad + \int_{kT_s}^{(k+1)T_s} \sum_{j=1}^{L}\sum_{i=0}^{M-1} C_{ni}^{(j)}\, g_j(t+mT_d-iT_d-\tau_j)u_0^*(t)\,dt \\ &\quad + \int_{kT_s}^{(k+1)T_s} v_n(t+mT_d)\,u_0^*(t)\,dt. \end{aligned} \tag{4.3}$$

In Appendix B it is shown that $y_{nm}(k)$ can be written explicitly in terms of the contributions of the designated user and the co-channel interference:

$$\begin{aligned} y_{nm}(k) &= A_0\, S_0(k)\, B_{nm(0)}^{(0)} + A_0\, S_0(k+1)\, B_{nm(1)}^{(0)} + A_0\, S_0(k-1)\, B_{nm(-1)}^{(0)} \\ &\quad + \sum_{j=1}^{L} \left[A_j\, S_j(k)\, B_{nm(0)}^{(j)} + A_j\, S_j(k+1)\, B_{nm(1)}^{(j)} + A_j\, S_j(k-1)\, B_{nm(-1)}^{(j)} \right] \\ &\quad + \eta_{nm}(k), \end{aligned} \tag{4.4}$$

where $B_{nm(\alpha)}^{(0)}$, $\alpha = (0, 1, -1)$ represents the aggregate cross-correlation with the designated user waveform $u_0(t)$ of all paths and symbols S_0, as seen at the mth tap delay in the nth channel. $B_{nm(\alpha)}^{(0)}$ consists of contributions of the current symbol $S_0(k)$, as well as the previous and the next symbols. Similarly, $B_{nm(\alpha)}^{(j)}$ represents contributions of the co-channel interferences $S_j(k+\alpha)$, $j = 1, \ldots, L$ to the output of the cross-correlation with $u_0(t)$. The term $\eta_{nm}(k)$ stands for the noise at the output of the matched filter. Consistent with the slow fading model assumed, all user and co-channel interference factors B are fixed during the processing interval. In this dissertation, we are concerned with the signal processing applied to the $y_{nm}(k)'s$, the

demodulated outputs of the array/tap-delay structure. The motivation for undertaking this effort is illustrated by Figure 4.1, which shows the eigenvalues of a sample covariance matrix of the space-time array for the case of 70 users. The covariance matrix was obtained by stacking the values y_{nm} and averaging over 50 symbols. The non-uniform distribution of the eigenvalues indicates that signal processing may be useful in improving the SNIR. Various space-time processing schemes are formulated in the next section.

4.2 Space-Time Combining Schemes

We consider two approaches to space-time processing: cascade space-time and joint domain processing. The cascade space-time processor consists of a temporal processor using the outputs of the spatial processor as shown in Figure 4.4. Processing could be MRC or optimum combining in each domain. The joint processor is applied simultaneously to all the signals in the array/tap-delay line structure. In the following, first the spatial combiner is defined, then it is used to formulate the cascade space-time configurations. The section concludes with the presentation of joint domain processing.

4.2.1 Spatial Combiner

Spatial processing combines the signals following spread spectrum demodulation, i.e., it combines the signals y_{nm} for each m. Unlike conventional phased arrays where a single (line-of-sight) path is assumed between the source and the array, our model assumes that each sensor receives signals independent of the other sensors. This can be achieved by allowing sufficient separation between sensors. Define the array vector at the output of the mth tap matched filter as $\mathbf{y}_m^T(k) = [y_{1m}(k), \ldots, y_{Nm}(k)]$. As can be seen from eq. (4.4), this output consists of the designated signal, interference and

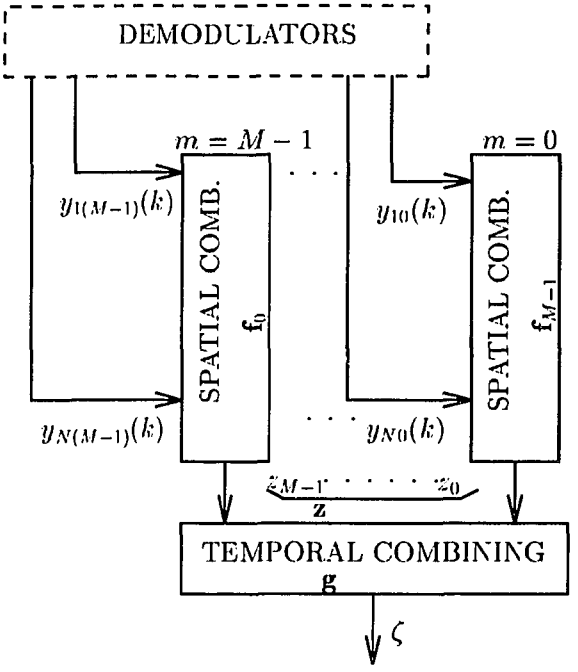

Figure 4.4 Configuration of cascade space-time processing

noise, and can be written:

$$\mathbf{y}_m(k) = A_0 S_0(k)\, \mathbf{B}^{(0)}_{m(0)} + \mathbf{I}_m + \mathbf{N}_m, \tag{4.5}$$

where $\mathbf{B}^{(0)}_{m(0)} = \left[B^{(0)}_{1m(0)}, \ldots, B^{(0)}_{Nm(0)}\right]^T$. This expression is similar in form to the output of a conventional phased array, with the random vector $\mathbf{B}^{(0)}_{m(0)}$ consisting of the transfer complex gain of the desired signal $S_0(k)$, from the source to each of the sensors. The interference vector can be expressed,

$$\mathbf{I}_m(k) = \sum_{j=0}^{L} \sum_{\substack{\alpha=-1 \\ \alpha,j\neq 0,0}}^{1} A_j S_j(k+i) \mathbf{B}^{(j)}_{m(\alpha)}. \tag{4.6}$$

Following spatial processing with the spatial weight vector $\mathbf{f}_m$, the array output at the mth tap-delay is given by $z_m(k) = \mathbf{f}_m^H \mathbf{y}_m(k)$.

With spatial MRC, each signal is weighted by the complex conjugate of the appropriate channel gain. The SMRC weight vector is given by:

$$\mathbf{f}_m = A_0 \mathbf{B}^{(0)}_{m(0)}, \tag{4.7}$$

for $0 \leq m \leq M-1$. Due to the independence between successive symbols of the same source, as well as the independence of the sources and the noise, the cross-correlation of the array vector and the desired signal is given by,

$$\begin{aligned} \mathbf{r}_m &= E[\mathbf{y}_m(k) S_o(k)] \\ &= A_0 \, \mathbf{B}^{(0)}_{m(0)}. \end{aligned} \tag{4.8}$$

Thus the SMRC weight vector is the cross-correlation, $\mathbf{f}_m = \mathbf{r}_m$. This observation suggests a practical way to compute $\mathbf{f}_m$ using a training sequence or previous bit estimates $\widehat{S}_o(k)$:

$$\hat{\mathbf{r}}_m = \frac{1}{K} \sum_{k=1}^{K} \mathbf{y}_m(k) \, \hat{S}_o(k). \tag{4.9}$$

The maximum ratio combiner optimizes the SNR but ignores the co-channel interference as well as the self-interference. The SNIR is optimized by the optimum combining weight vector:

$$\mathbf{f}_m = \mathbf{R}_m^{-1} \mathbf{r}_m, \tag{4.10}$$

where $\mathbf{R}_m$ is the array interference and noise covariance matrix at the output of the mth correlator and is defined by:

$$\mathbf{R}_m = E\left\{ \left[\mathbf{y}_m(k) - S_o(k)\mathbf{r}_m\right] \left[\mathbf{y}_m(k) - S_o(k)\mathbf{r}_m\right]^H \right\}. \tag{4.11}$$

This covariance matrix can be estimated similar to the cross-correlation vector:

$$\widehat{\mathbf{R}}_m = \frac{1}{K} \sum_{k=1}^{K} \left[\mathbf{y}_m(k) - \widehat{S}_o(k)\hat{\mathbf{r}}_m\right] \left[\mathbf{y}_m(k) - \widehat{S}_o(k)\hat{\mathbf{r}}_m\right]^H. \tag{4.12}$$

4.2.2 Space-Time Combiner

Let $\mathbf{z}^T(k) = [z_1(k), \ldots, z_M(k)]$ be a vector that consists of the M outputs of the spatial combiners. The vector $\mathbf{z}(k)$ is fed into the temporal combiner. It can be expressed:

$$\mathbf{z}(k) = A_0 \, S_0(k) \, \mathbf{H} + \mathbf{I}_t + \mathbf{N}_t, \tag{4.13}$$

where $\mathbf{H}^T = \left[\mathbf{f}_0^H \mathbf{B}_{1(0)}^{(0)}, \ldots, \mathbf{f}_{M-1}^H \mathbf{B}_{M-1,(0)}^{(0)}\right]$, $\mathbf{I}_t^T = \left[\mathbf{f}_0^H \mathbf{I}_0, \ldots, \mathbf{f}_{M-1}^H \mathbf{I}_{M-1}\right]$, and $\mathbf{N}_t^T = \left[\mathbf{f}_0^H \mathbf{N}_0, \ldots, \mathbf{f}_{M-1}^H \mathbf{N}_{M-1}\right]$. The output of the space-time combiner is given by $\varsigma(k) = \mathbf{g}^H \mathbf{z}(k)$, where $\mathbf{g}$ is the temporal weight vector. The weight vector $\mathbf{g}$ is derived similar to the spatial weight vectors $\mathbf{f}_m$. Several space-time cascade configurations are considered. (For acronyms, please refer to the introduction.) The SMRC/TMRC configuration is defined by

$$\mathbf{g} = \mathbf{H}, \tag{4.14}$$

where in the definition of $\mathbf{H}$, the spatial weight vectors $\mathbf{f}_m$ are given by eq. (4.7). Assuming independence between the various random variables, the cross-correlation between the space-time combiner output and the desired signal is given by

$$\begin{aligned} \mathbf{r}_t &= E[\mathbf{z}(k) S_o(k)] \\ &= A_0 \mathbf{H}. \end{aligned} \tag{4.15}$$

Therefore, the TMRC weight vector can be found from the estimate of the cross-correlation vector. With the SOPT/TMRC configuration, the SNIR at the output of the temporal processor is maximized by the optimum weight vector,

$$\mathbf{g} = \mathbf{R}_t^{-1} \mathbf{r}_t, \tag{4.16}$$

where $\mathbf{R}_t$ is the array interference and noise covariance matrix at the input of the temporal combiner and is given by

$$\mathbf{R}_t = E\left[\left(\mathbf{z}(k) - S_o(k)\mathbf{r}_t\right)\left(\mathbf{z}(k) - S_o(k)\mathbf{r}_t\right)^H\right]. \tag{4.17}$$

The previous relation suggests a practical way of estimating the interference covariance matrix by substituting for $S_o(k)$ and $\mathbf{r}_t$ previous symbol and cross-correlation vector estimates. Table 4.1 summarizes the space-time receiver configurations.

The SNIR at the output of the space-time combiner is given by the expression:

$$\rho = \frac{E_b}{I_o + N_o} = \frac{A_0^2 E\left[\left|\mathbf{g}^H \mathbf{H}\right|^2\right]}{E\left[\left|\mathbf{g}^H \mathbf{I}_t\right|^2\right] + E\left[\left|\mathbf{g}^H \mathbf{N}_t\right|^2\right]}, \tag{4.18}$$

Spatial Proc.	Temporal Proc.	Space-Time
$\mathbf{f}_m = \mathbf{r}_m$ (SMRC)	$\mathbf{g} = \mathbf{H}$ (TMRC)	SMRC/TMRC
$\mathbf{f}_m = \mathbf{R}_m^{-1}\mathbf{r}_m$ (SOPT)	$\mathbf{g} = \mathbf{H}$ (TMRC)	SOPT/TMRC
$\mathbf{f}_m = \mathbf{R}_m^{-1}\mathbf{r}_m$ (SOPT)	$\mathbf{g} = \mathbf{R}_t^{-1}\mathbf{r}_t$ (TOPT)	SOPT/TOPT

Table 4.1 Cascade space-time receiver configurations

where E_b is the bit energy, I_o is the interference power spectral density and N_o is the noise power spectral density. The expectation is taken with respect to the noise over a time interval during which the channel is considered constant. Thus, ρ is viewed as a random variable and is a function of the channel parameters $B_{nm(\alpha)}^{(j)}$, the source power P_j, and the voice activity ψ_j. The conditional bit error rate (BER) is given by

$$P_{e|\rho} = Q\left(\sqrt{2\rho}\right). \tag{4.19}$$

It is common to evaluate the system performance in terms of the outage, defined as the probability of the BER exceeding a set level. To derive an expression for the outage, consider the various components of ρ. The bit energy E_b can be set to 1, without affecting the SNIR, by suitable scaling of the weight vector $\mathbf{g}$. The interference and noise, $I_o + N_o$ term, is the aggregate of a large number of independent sources, symbols and noise. Hence, according to the central limit theorem, it may be regarded as a normal random variable with some mean μ_I and variance σ_I^2. The outage can then be calculated from [5],

$$\Pr\left[\frac{E_b}{I_o + N_o} \leq \xi\right] = Q\left(\frac{1/\xi - \mu_I}{\sigma_I}\right). \tag{4.20}$$

4.2.3 Joint-Domain Combiner

With the joint domain combiner, processing occurs jointly in the space-time domains. To formulate the weight vectors of the joint domain combiner, define the NM-

dimensional stacked vector after spread spectrum demodulation:

$$\begin{aligned} \mathbf{Y}(k) &= \left[\mathbf{y}_0^T(k), \ldots, \mathbf{y}_{M-1}^T(k)\right]^T \\ &= A_0 S_0(k)\,\mathbf{B}_0 + \mathbf{I}(k) + \mathbf{N}(k), \end{aligned} \tag{4.21}$$

where $\mathbf{B}_o^T = \left[\mathbf{B}_{0(0)}^{(0)T}, \ldots, \mathbf{B}_{M-1,(0)}^{(0)T}\right]$, $\mathbf{I}^T(k) = \left[\mathbf{I}_0^T(k), \ldots, \mathbf{I}_{M-1}^T(k)\right]$, and $\mathbf{N}^T(k) = \left[\mathbf{N}_0^T(k), \ldots, \mathbf{N}_{M-1}^T(k)\right]$. The joint domain cross-correlation vector and the space-time covariance matrix are given by

$$\mathbf{r} = E[\mathbf{Y}(k)S_o(k)] = A_o\mathbf{B}_o \tag{4.22}$$

and

$$\begin{aligned} \mathbf{R} &= E[(\mathbf{I}(k) + \mathbf{N}(k))(\mathbf{I}(k) + \mathbf{N}(k))^H] \\ &= E[(\mathbf{Y}(k) - S_o(k)\mathbf{r})(\mathbf{Y}(k) - S_o(k)\mathbf{r})^H], \end{aligned} \tag{4.23}$$

respectively. The JMRC weight vector is given by $\mathbf{w} = \mathbf{r}$. It is readily shown that, with proper scaling, the SMRC/TMRC and JMRC configurations provide exactly the same outputs. The cascade and joint configurations, however, do not provide the same performance when optimum processing is applied. This is illustrated in the next section. The JOPT weight vector is given by

$$\mathbf{w} = \mathbf{R}^{-1}\mathbf{r}. \tag{4.24}$$

The difference in performance between the cascade and the joint domain weight vectors is a consequence of the number of degrees of freedom available to each configuration. The cascade configuration has $(N + M - 2)$ degrees of freedom while the joint domain configuration has $(NM - 1)$ degrees of freedom. In a typical CDMA scenario, the number of interferences $L \gg NM$ and each interference has multipath as well, hence each additional degree of freedom provides increased performance. The outage for joint domain processing is evaluated using the following SNIR expression:

$$\rho = \frac{E_b}{I_o + N_o} = \frac{A_0^2 E\left[\left|\mathbf{w}^H\mathbf{B}_0\right|^2\right]}{E\left[\left|\mathbf{w}^H\mathbf{I}\right|^2\right] + E\left[\left|\mathbf{w}^H\mathbf{N}\right|^2\right]}. \tag{4.25}$$

4.3 Numerical Results

This section presents numerical results on the performance of the configurations studied in the previous section. Both perfect and imperfect power control are considered, and the effect of the number of antennas on the BER and outage probability is studied. The scenario is typical to communications using the existing IS-95 CDMA standard. Based on a multipath coherence bandwidth of 300 kHz and a CDMA signal bandwidth of 1.25 MHz., the channel was modeled with four taps. The information symbols were modulated by Gold sequences of length 127. The SNR before spread spectrum demodulation was set to 0.8. For the case of perfect power control, all sources were assumed to have the same power as the desired signal. The case of imperfect power control was modeled using the approach taken in [32]. For the maximum allowed fractional deviation ϵ, the PCE was modeled as uniformly distributed between $1-\epsilon$ and $1+\epsilon$. The standard deviation of the PCE is then $\sigma_{\text{PCE}} = \sqrt{\epsilon}$. Thus, a standard deviation of 2 dB corresponds to $\epsilon = 0.4$. Covariance matrices and cross-correlation vectors were estimated from blocks of 50 symbols using relations similar to those in eqs. (4.12) and (4.9), respectively. Curves, shown in Figures 4.5 to 4.10, are obtained by using eqs. (4.19) and (4.20) and are averages of 100 Monte Carlo runs.

Figures 4.5 and 4.6 show the BER and outage, respectively, as a function of the capacity for the different space-time configurations and for $N = 1, 2$ antennas. The power control was assumed perfect. Figure 4.5 indicates that at a probability of symbol error of 10^{-3} and for $N = 1$, optimal processing increases capacity by close to 30% over diversity processing only (the conventional RAKE receiver). For $N = 2$, JOPT increases capacity from 85 to 125 users. In Figure 4.6 it is shown that with JOPT, the capacity, measured at an outage of 10^{-3}, is increased from 20 to 30 for a single antenna, and from 45 to 65 for two antennas. Note that this improvement comes at a relatively small increase in complexity since,

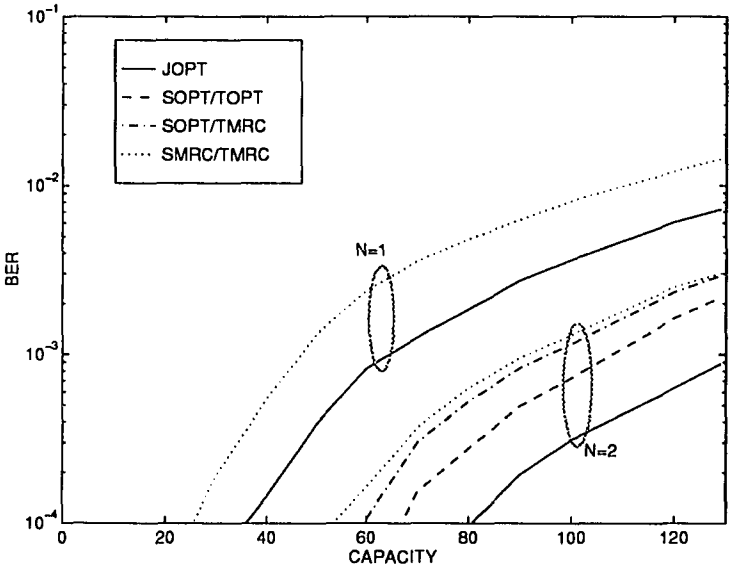

Figure 4.5 BER vs. capacity with perfect power control

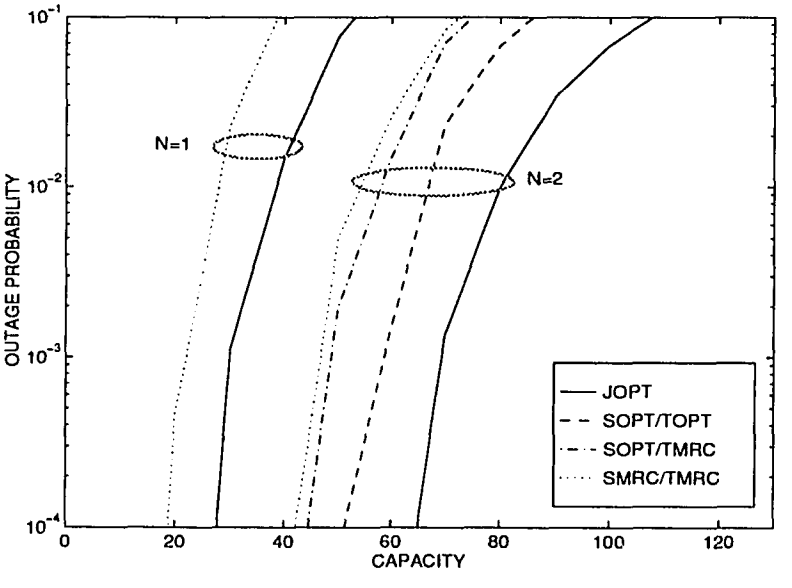

Figure 4.6 Outage probability vs. capacity with perfect power control

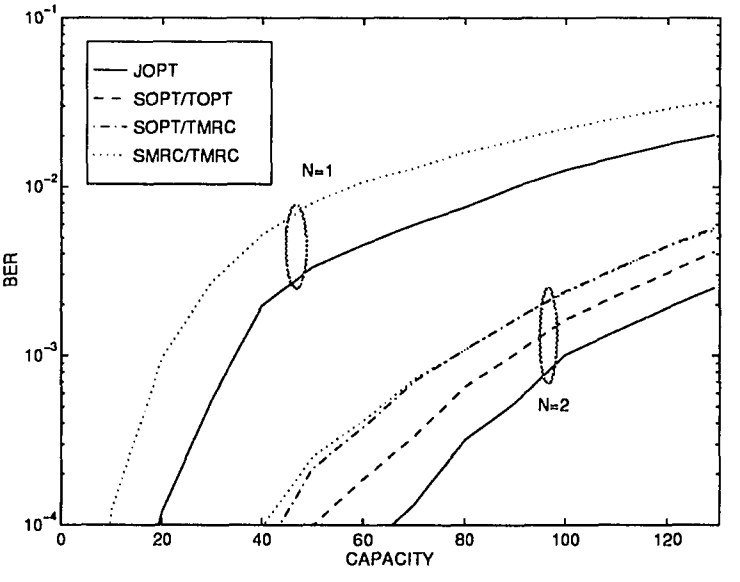

Figure 4.7 BER vs. capacity with PCE=2 dB

while optimum combining requires matrix inversion, the matrix dimension is not large. The configuration SOPT/TMRC provides only little improvement. Thus, both JOPT and SOPT/TOPT are superior to SOPT/TMRC. This is not surprising since for two antennas there is only a single degree of freedom to exploit. The capacity of the SOPT/TOPT configuration is about half-way between the capacities of the SMRC/TMRC and JOPT configurations. It should be noted however, that these results represent the steady state system performance. It is possible that the adaptation of the larger number of degrees of freedom associated with the JOPT structure may require longer settling times or, equivalently, longer training sequences than the cascade configurations. This may make the joint domain configuration more sluggish to respond to changes in the signal environment due to sudden changes (such as a user entering or leaving). Trade-offs between the transient and steady states will be considered in our future work.

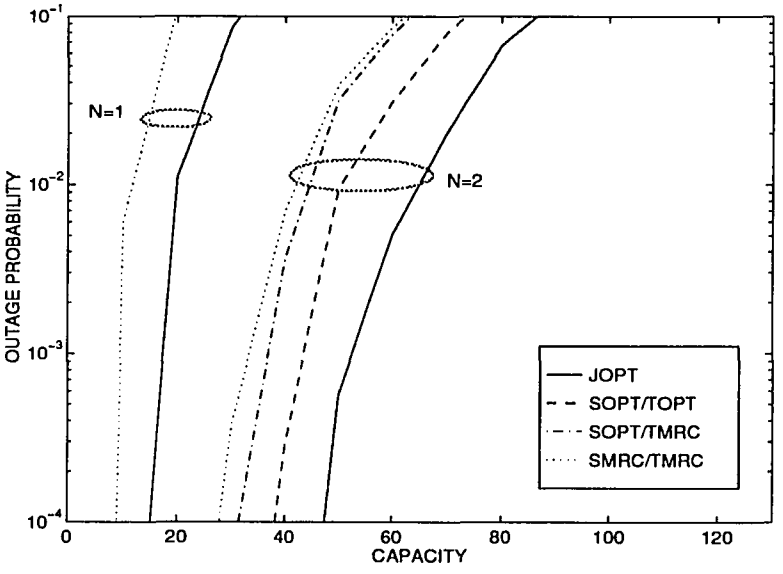

Figure 4.8 Outage probability vs. capacity with PCE=2 dB

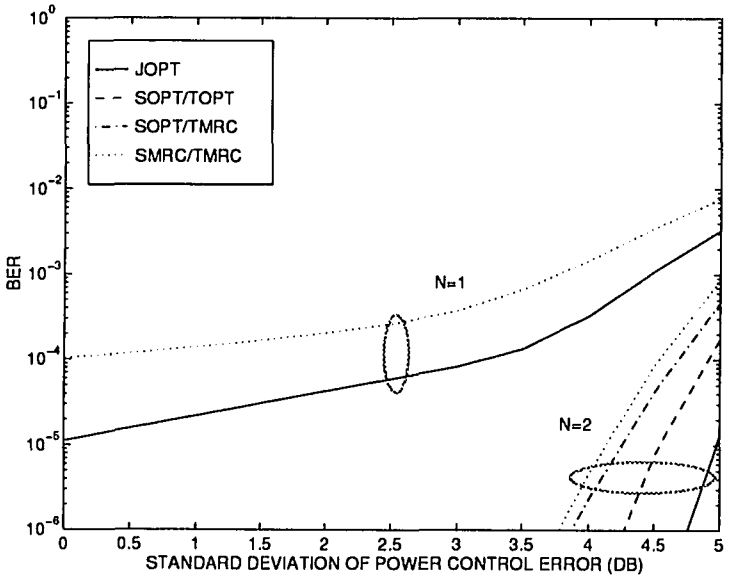

Figure 4.9 BER vs. power control error for K=10 users

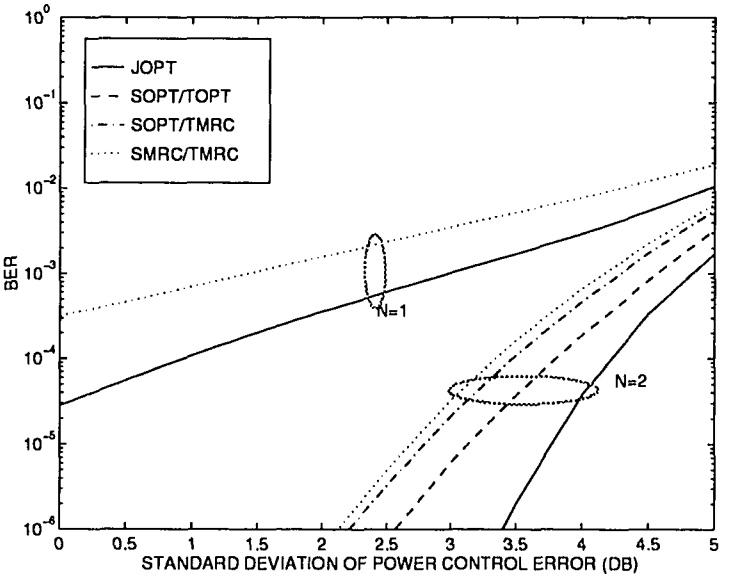

Figure 4.10 BER vs. power control error for K=20 users

The effect of imperfect power control on capacity can be assessed from Figures 4.7 and 4.8. It is observed that a 2 dB PCE generally causes a significant drop in capacity for each configuration. Optimum combining can thus be viewed as providing a trade-off to power control. This is illustrated in Figures 4.9 and 4.10, which show the effect of the PCE on the BER. For example, from Figure 4.10, it is observed that for BER = 10^{-5} and $N = 2$, JOPT provides a margin of about 1 dB PCE over SMRC/TMRC.

The previous results are based on the gaussian assumption of MAI, so that $Q(.)$ function can be used to evaluate the system performance as of eqs. (4.19) and (4.20). In order to verify this assumption, we run simulations to count the bit error rate over 12,000 bits at each point as shown in Figure 4.11. The simulation points match the curves.

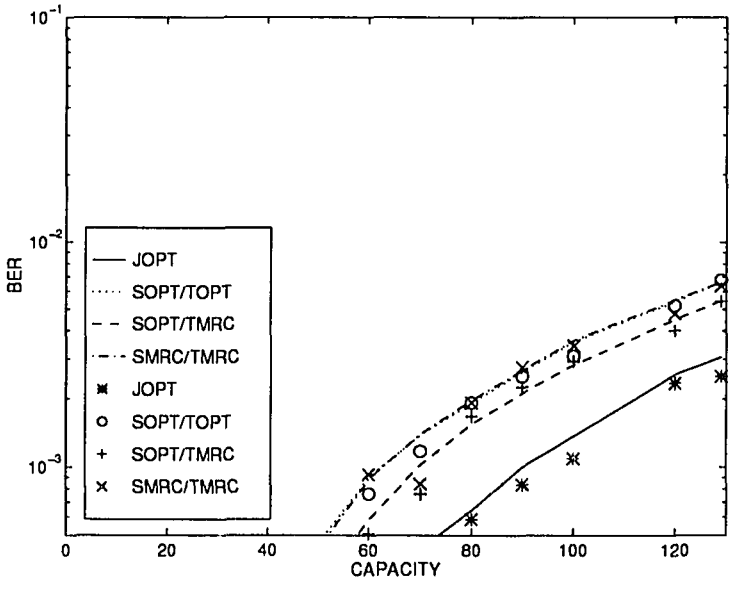

Figure 4.11 BER verification with N=2 antennas and PCE=2 dB

4.4 Near-Far Resistance

According to Appendix B equation B.2, the output of the demodulator has the following approximation

$$\begin{aligned} \mathbf{Y}(k) &= A_o S_o(k)\mathbf{B}_o + \mathbf{I}(k) + \mathbf{N}(k) \\ &\approx A_o D S_o(k)\mathbf{C} + \mathbf{I}(k) + \mathbf{N}(k), \end{aligned} \tag{4.26}$$

assuming inter-path contributions are small. $\mathbf{C} = [C_{10}^{(0)}, \ldots, C_{N(M-1)}^{(0)}]$ is the channel coefficient vector of the desired user. To simplify the analysis, we define the normalized channel vector $\mathbf{C} = \mathbf{c}/|\mathbf{c}|$ such that the array processing gain $|\mathbf{C}| = 1$. The space-time processor's output is given by

$$\zeta = \mathbf{w}^H\mathbf{Y} = A_o D S_o(k)\mathbf{w}^H\mathbf{C} + \mathbf{w}^H\mathbf{I}(k) + \mathbf{w}^H\mathbf{N}(k). \tag{4.27}$$

From eq. (B.9), the noise covariance matrix is given by $E[\mathbf{N}(k)\mathbf{N}(k)^H] = D\sigma_v I$, where I is the identity matrix. The worst case is when all interferences combine to reduce the output due to the desired signal. We have the minimum SNR at the output

$$(SNR)_{min} = E\left[\frac{(A_o D|\mathbf{w}^H\mathbf{C}| - |\mathbf{w}^H\mathbf{I}(k)|)^2}{D\sigma_v^2|\mathbf{w}|^2}\right]. \tag{4.28}$$

The $(SNR)_{min}$ determines the probability of error P_e for the desired user. To achieve this error probability P_e, the SNR at the input of space-time processor or the output of the demodulator is required as follows:

$$(SNR)_{in} = \frac{A_o^2 D^2}{D\sigma_v^2} = \frac{A_o^2 D}{\sigma_v^2}, \tag{4.29}$$

The *effective* SNR is defined as the SNR in a way that the desired user would require to achieve the error probability P_e in the same Gaussian channel but without interferences. In this case, we get *effective* $(SNR)_e = (SNR)_{min}$. The *asymptotic efficiency* is defined as the ratio $(SNR)_e/(SNR)_{in}$ in the region of low noise power which can be written as follows:

$$\eta = \frac{(SNR)_e}{(SNR)_{in}} = E\left\{\frac{\left[\max\left(0, |\mathbf{w}^H\mathbf{C}| - \frac{|\mathbf{w}^H\mathbf{I}(k)|}{A_o D}\right)\right]^2}{|\mathbf{w}|^2}\right\}. \tag{4.30}$$

Notice that in the absence of interferences ($\mathbf{I}(k) = 0$) and since $|\mathbf{C}| = 1$, the asymptotic efficiency equals to 1 ($\eta = 1$).

Let us consider one interference synchronized case. There, the interference term can be written as $\mathbf{I}(k) \approx A_I S_I(k)\mathbf{C}_I$, where $\mathbf{C}_I$ is the normalized channel coefficient vector of the interference user with $|\mathbf{C}_I| = 1$. The MRC method yields the weight vector $\mathbf{w}_m = \mathbf{C}$, so that the asymptotic efficiency is given by:

$$\eta_{mrc} = E\left\{\left[\max\left(0, 1 - \frac{A_I}{A_o D}|\mathbf{C}^H\mathbf{C}_I|\right)\right]^2\right\}. \tag{4.31}$$

In Appendix C, it is shown that $E\left[|\mathbf{C}^H\mathbf{C}_I|\right] = \sqrt{\pi/(4NM)}$, and $E\left[|\mathbf{C}^H\mathbf{C}_I|^2\right] = 1/(NM)$. Further simplifying eq. (4.31), we get

$$\eta_{mrc} \approx \left[\max\left(0, 1 - \sqrt{\frac{\pi}{NM}} \cdot \frac{A_I}{2A_oD}\right)\right]^2 \tag{4.32}$$

When the interference power increases, the asymptotic efficiency decreases until it vanishes. Hence, the MRC is not near-far resistant.

With optimum combining the weight vector is given by $\mathbf{w}_o = \mathbf{R}_n^{-1}\mathbf{C}$, where $\mathbf{R}_n = A_I^2\mathbf{C}_I\mathbf{C}_I^H + D\sigma_v^2\mathbf{I}$. Using the matrix inversion lemma, $\mathbf{R}_n^{-1} = \left(\mathbf{I} - \alpha\mathbf{C}_I\mathbf{C}_I^H\right)/(D\sigma_v^2)$, where $\alpha = A_I^2/(D\sigma_v^2 + A_I^2)$. The asymptotic efficiency of optimum combining can be written as follows:

$$\eta_{opt} = E\left[\frac{\left(1 - \alpha|\mathbf{C}^H\mathbf{C}_I|^2 - \frac{\alpha\sigma_v^2}{A_oA_I}|\mathbf{C}^H\mathbf{C}_I|\right)^2}{1 - \alpha(2-\alpha)|\mathbf{C}^H\mathbf{C}_I|^2}\right]. \tag{4.33}$$

In the region of low noise power, we have $\alpha \to 1$ and $\alpha\sigma_v^2/(A_oA_I) \to 0$ so that the asymptotic efficiency of optimum combining can be further simplified as follows:

$$\begin{aligned}\eta_{opt} &= E\left[1 - |\mathbf{C}^H\mathbf{C}_I|^2\right] \\ &= 1 - \frac{1}{NM}.\end{aligned} \tag{4.34}$$

It means that space-time processing with the optimum combining is near-far resistant in the one interference case.

Figure 4.12 shows the asymptotic efficiency of an adaptive array for two synchronized users with spread gain $D = 127$, system dimension $NM = 5$ and $NM = 8$. Both simulation results and theory calculations show that the optimum combining is near-far resistant while MRC is not. The simulation curves were obtained by using eq. (4.30) and averaging over 1000 runs while the theory curves for the MRC and the optimum combining were obtained by using eq. (4.32) and eq. (4.34), respectively.

When the number of the interferences, (which include delayed version of multipaths), is smaller than the system dimension, optimum combining has sufficient

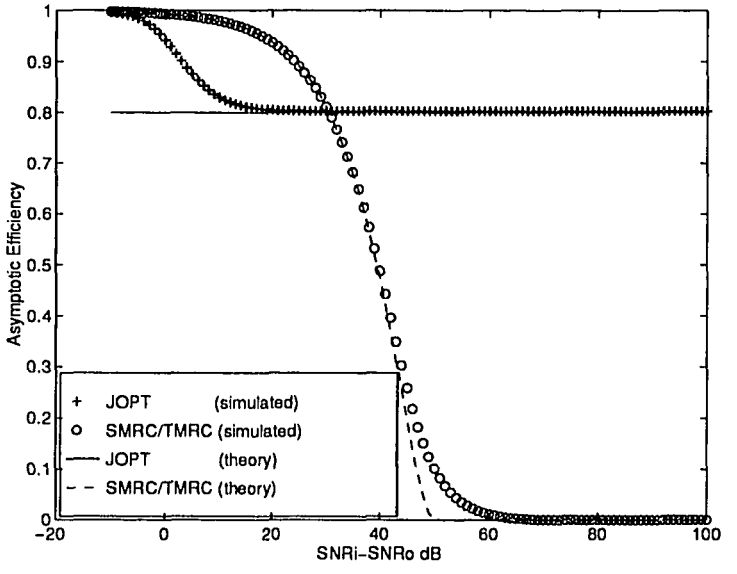

(a) NM=5

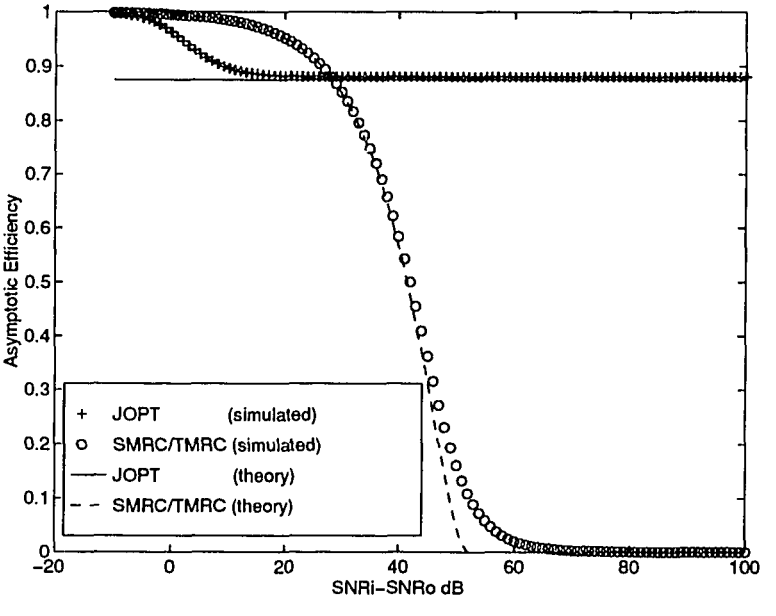

(b) NM=8

Figure 4.12 Asymptotic efficiency of an adaptive array for two users with (a) NM=5, (b) NM=8

degrees of freedom to null all interferences making the system near-far resistant. When the number of the interferences is larger than the system dimension, optimum combining cannot null all the interferences and the system ceases to be near-far resistant.

4.5 Summary

In this chapter, we studied space-time processing for CDMA-based wireless communications. Specifically, the following configurations were suggested: (1) space-time diversity, (2) cascade optimum spatial-diversity temporal (RAKE), (3) cascade optimum spatial-optimum temporal, and (4) joint domain optimum processing. We considered a typical CDMA wireless communications scenario modeled by a four tap-delay line and showed that a two-antenna system provides double the capacity of a single antenna system. Joint domain optimum combining provides an additional 25% increase in capacity over diversity processing only. It also provides a 1 dB power control error margin over MRC. These improvements come at only modest cost due to the few degrees of freedom that need to be optimized. We conclude that joint space-time optimum combining is a cost-efficient method for increasing capacity of CDMA-based wireless communications.

CHAPTER 5

CONCLUSIONS

In this dissertation, we have studied space-time processing to increase wireless communication systems capacity and improve their performance.

In Chapter 2, adaptive spatial processing to increase TDMA system capacity has been studied. The estimation of an array covariance matrix entails a loss in the array output SNIR with respect to the optimal case of a known covariance matrix. The density function of this loss has been derived elsewhere for both the DMI and the eigencanceler methods and is used to develop an analytical expression for the average probability of error for each method for single interference. It is shown that the eigencanceler method has performance close to the optimal in some case and is superior to the performance of the DMI method in some case. Simulations are used to corroborate the analytical results. In Chapter 3, we presented the implementation of the eigencanceler by using a simple projection-based algorithm.

In Chapter 4, we studied space-time processing for CDMA-based wireless communications. Specifically, the following configurations were suggested: (1) space-time diversity, (2) cascade optimum spatial-diversity temporal (RAKE), (3) cascade optimum spatial-optimum temporal, and (4) joint domain optimum processing. We considered a typical CDMA wireless communications scenario modeled by a four tap-delay line and showed that a two-antenna system provides double the capacity of a single antenna system. Joint domain optimum combining provides an additional 25% increase in capacity over diversity processing only. It also provides a 1 dB power control error margin over MRC. These improvements come at only modest cost due to the few degrees of freedom that need to be optimized. We conclude that joint space-time optimum combining is a cost-efficient method for increasing capacity of CDMA-based wireless communications.

APPENDIX A

CALCULATION OF INTEGRAL TERM

In this appendix, we evaluate the integral term of eq. 2.13. Let $c = -(\gamma_o|A_1|^2/|A_s|^2)N)$, so that

$$\int_0^1 e^{-(\gamma_o|A_1|^2/|A_s|^2)Nt}(1-t)^{N-2}dt = \int_0^1 e^{ct}(1-t)^{N-2}dt. \tag{A.1}$$

Defining

$$y(N-2) = \int_0^1 e^{ct}(1-t)^{N-2}dt, \tag{A.2}$$

we get

$$\begin{aligned} y(N) &= \int_0^1 e^{ct}(1-t)^N dt \\ &= \frac{1}{c}\int_0^1 (1-t)^N de^{Nt} \\ &= \frac{1}{c}\left[(1-t)^N e^{ct}|_0^1 + \int_0^1 e^{ct}N(1-t)^{N-1}dt\right] \\ &= \frac{1}{c}\left[-1 + N\int_0^1 e^{ct}(1-t)^{N-1}dt\right]; \end{aligned} \tag{A.3}$$

hence

$$y(N) = -\frac{1}{c} + \frac{N}{c}y(N-1) \tag{A.4}$$

and

$$y(0) = \int_0^1 e^{ct}dt = \frac{e^c - 1}{c}. \tag{A.5}$$

APPENDIX B

CORRELATION OF CDMA SIGNALS

This appendix evaluates the terms of eq. 4.3. This relation represents the correlation of the signal received at the mth tap-delay with the signature waveform of the designated user. Let the three terms on the right-hand side of eq. 4.3 be denoted T_1, T_2 and T_3, respectively. T_1 represents the aggregate contributions of the designated user at the mth tap-delay. It can be further analyzed as follows:

$$T_1 = A_0 S_0(k) B^{(0)}_{nm(0)} + A_0 S_0(k+1) B^{(0)}_{nm(1)} + A_0 S_0(k-1) B^{(0)}_{nm(-1)}, \tag{B.1}$$

where the factor $B^{(0)}_{nm(0)}$ represents contributions of $S_0(k)$ to the output of the matched filter at the nth element and mth tap-delay. This factor consists of the correlation of the desired signal in the mth path with the signature waveform $u_0(t)$, as well as inter-path contributions, and can be written,

$$B^{(0)}_{nm(0)} = C^{(0)}_{nm} \rho_{00}(0, 0, T_s) + b^{(0)}_{nm}, \tag{B.2}$$

where $\rho_{jl}(\tau, t_1, t_2)$ is the partial correlation between the signature waveforms of users j and l, with time lag τ between the waveforms, and time limits t_1 and t_2:

$$\rho_{jl}(\tau, t_1, t_2) = \int_{t_1}^{t_2} u_j(\alpha + \tau) u_l^*(\alpha) d\alpha. \tag{B.3}$$

Note that $\rho_{00}(0, 0, T_s) = D$, the processing gain, as expected. The complex normal variable $b^{(0)}_{nm}$ (constant during the processing interval) represents the contributions of $S_0(k)$ paths other than the mth. It consists of paths, $i < m$, that arrive prior to path m, and paths, $i > m$, that arrive after m. It is given by:

$$b^{(0)}_{nm} = \sum_{i=0}^{m-1} C^{(0)}_{ni} \rho_{00}[(m-i)T_d, 0, T_s - (m-i)T_d] + \sum_{i=m+1}^{M-1} C^{(0)}_{ni} \rho_{00}[(m-i)T_d, (i-m)T_d, T_s]. \tag{B.4}$$

A timeline diagram is provided in Figure B.1 to clarify the time limits used in the various correlation expressions. Factors of the form $B^{(0)}_{nm(\alpha)}$, $\alpha = -1, 1$ represent

contributions associated with the $(k+\alpha)$th symbol of the designated user. Note that the mth path waveform of $S_0(k)$ may overlap with the $i < m$th path waveform of the next symbol $S_0(k+1)$ or with the $i > m$th path waveform of the previous symbol $S_0(k-1)$. This factor can be explicitly written

$$\begin{aligned} B^{(0)}_{nm(0)} &= C^{(0)}_{nm}\,\rho_{00}(0,0,T_s) + b^{(0)}_{nm} \\ B^{(0)}_{nm(1)} &= \textstyle\sum_{i=0}^{m-1} C^{(0)}_{ni}\,\rho_{00}[(m-i)T_d,(i-m)T_d,0] \\ B^{(0)}_{nm(-1)} &= \textstyle\sum_{i=m+1}^{M-1} C^{(0)}_{ni}\,\rho_{00}[(m-i)T_d,0,(i-m)T_d]. \end{aligned} \tag{B.5}$$

The time limits of the correlations can be visualized using Figure B.1 and noting the periodicity of $u_0(t)$.

The term T_2 represents the co-channel interference. It is given by

$$T_2 = \sum_{j=1}^{L}\left[A_j\,S_j(k)\,B^{(j)}_{nm(0)} + A_j\,S_j(k+1)\,B^{(j)}_{nm(1)} + A_j\,S_j(k-1)\,B^{(j)}_{nm(-1)}\right]. \tag{B.6}$$

With some considerable algebraic manipulations, but in a manner similar to the derivation of eq. B.5, it can be shown that the terms $B^{(j)}_{nm(\alpha)}, \alpha = -1,0,1$ are given by:

$$\begin{aligned} B^{(j)}_{nm(0)} &= C^{(j)}_{n(m-\lfloor T_j/T_d\rfloor)}\rho_{0m}(0,0,T_s) + b^{(j)}_{nm} \\ B^{(j)}_{nm(1)} &= \textstyle\sum_{i=0}^{m-\lfloor T_j/T_d\rfloor-1} C^{(j)}_{ni}\,\rho_{j0}[(m-i)T_d-\tau_j,(i-m)T_d+\tau_j,0] \\ B^{(j)}_{nm(-1)} &= \textstyle\sum_{i=m-\lfloor T_j/T_d\rfloor+1}^{M} C^{(j)}_{ni}\,\rho_{j0}[(m-i)T_d-\tau_j,0,(i-m)T_d+\tau_j], \end{aligned} \tag{B.7}$$

where

$$\begin{aligned} b^{(j)}_{nm} &= \sum_{i=0}^{m-\lfloor T_j/T_d\rfloor-1} C^{(j)}_{ni}\,\rho_{j0}[(m-i)T_d-\tau_j,(i-m)T_d+T_j,0] \\ &\quad + \sum_{i=m-\lfloor T_j/T_d\rfloor+1}^{M} C^{(j)}_{ni}\,\rho_{j0}[(m-i)T_d-\tau_j,0,(i-m)T_d+\tau_j,T_s]. \end{aligned} \tag{B.8}$$

Finally, T_3 is the noise after matched filtering:

$$\eta_{nm}(k) = \int_{kT_s}^{(k+1)T_s} v_n(t+mT_d)\,u_0^*(t)\,dt,$$

where the noise variance is given;

$$\sigma_\eta^2 = D\sigma_v^2. \tag{B.9}$$

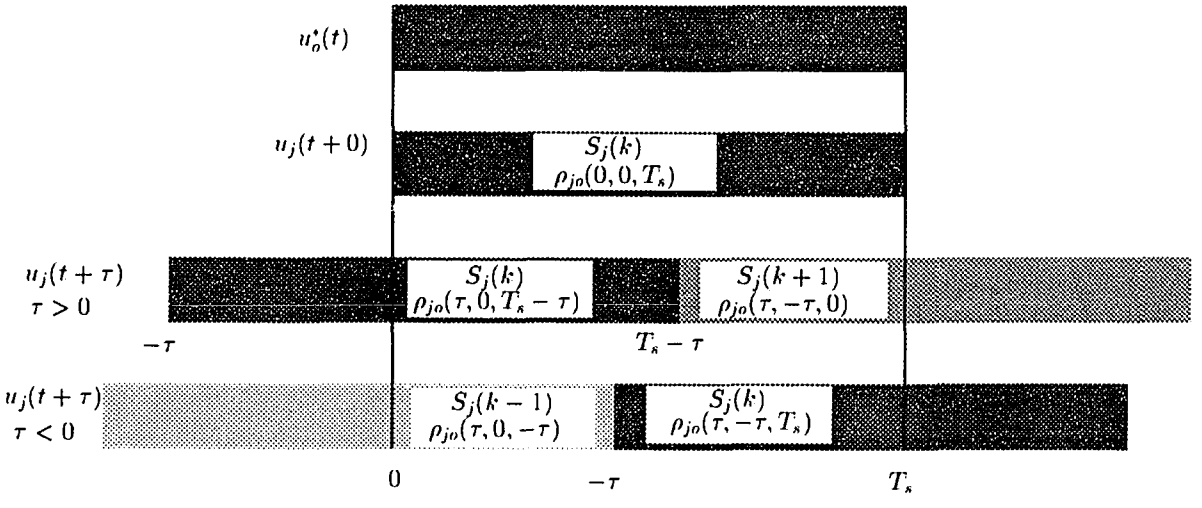

Figure B.1 Timeline for correlation calculations

APPENDIX C

CORRELATION OF CHANNEL COEFFICIENTS

This appendix evaluates the first and second moment of the random variable $|\mathbf{C}^H\mathbf{C}_I|$ — the amplitude of the correlation of channel coefficient vectors. In the context of Section 4.4,the channel coefficients are normalized to preclude their effect of the processing gain. $\mathbf{C}$ and $\mathbf{C}_I$ can be modeled as normalized complex Gaussian vectors with zero means and unit norms:

$$\mathbf{C} = [C_1 \dots C_{NM}]^T = \frac{\mathbf{c}}{|\mathbf{c}|} \tag{C.1}$$

$$\mathbf{C}_I = [C_{I1} \dots C_{INM}]^T = \frac{\mathbf{c}_I}{|\mathbf{c}_I|}, \tag{C.2}$$

where $\mathbf{c}$ and $\mathbf{c}_I$ are random vectors with elements $c_n = c_{nr} + jc_{ni}$ and $c_{In} = c_{Inr} + jc_{Ini}$. Coefficients c_{nr}, c_{Inr} and c_{ni}, c_{Ini} are real and imaginary parts of the elements c_n and c_{In}, respectively, and are i.i.d random variables with distribution $N(0, \sigma_c/\sqrt{2})$. Hence, random variables $|C_n|^2$ can be written as follows:

$$|C_n|^2 = \frac{c_{nr}^2 + c_{ni}^2}{(c_{nr}^2 + c_{ni}^2) + \sum_{k=1,k\neq n}^{NM}(c_{kr}^2 + c_{ki}^2)}. \tag{C.3}$$

From eq. (C.3), we can notice that $|C_n|^2$ has beta distributions with 2 and $2(NM-1)$ degrees of freedom. $|C_{In}|^2$ has the same distribution as well. The mean of these random variable is given:

$$E\left[|C_n|^2\right] = E\left[|C_{In}|^2\right] = \frac{1}{NM}. \tag{C.4}$$

Let

$$x_n = x_{nr} + jx_{ni} = C_n^* C_{In}, \tag{C.5}$$

where x_{nr} and x_{ni} are the real and imaginary parts of x_n. Both are independent random variables with means and second moments given as follows:

$$E[x_{nr}] = E[x_{ni}] = E[x_n] = 0 \tag{C.6}$$

$$E[x_{nr}^2] = E[x_{ni}^2] = \frac{1}{2}E[|x_n|^2] = \frac{1}{2(NM)^2}. \tag{C.7}$$

We form their sum

$$\begin{aligned} \mathcal{Z} &= \mathcal{Z}_r + j\mathcal{Z}_i \\ &= x_1 + \ldots + x_{NM} \\ &= \mathbf{C}^H \mathbf{C}_I, \end{aligned} \tag{C.8}$$

where $\mathcal{Z}_r$ and $\mathcal{Z}_i$ are the real and imaginary parts of $\mathcal{Z}$. According to the central limit theorem, $\mathcal{Z}_r$ and $\mathcal{Z}_i$ have normal distributions $N(0, \sqrt{1/(2NM)})$. Hence, the amplitude of the random variable $\mathcal{Z}$ has Rayleigh distribution with mean

$$E[|\mathcal{Z}|] = \sqrt{\frac{\pi}{4NM}} \tag{C.9}$$

and variance

$$E[(|\mathcal{Z}| - E[|\mathcal{Z}|])^2] = \frac{4-\pi}{4NM}. \tag{C.10}$$

Thus, we have

$$E[|\mathcal{Z}|^2] = \frac{1}{NM}. \tag{C.11}$$

APPENDIX D

GLOSSARY OF ABBREVIATIONS

AMPS: advanced mobile phone system

CDMA: code-division multiple-access

CIR: carrier-to-interference ratio

DMI: direct matrix inverse

EVD: eigenvalue decomposition

FDMA: frequency-division multiple-access

GSM: global system for mobile communications

JOPT: joint domain optimum combining

LMS: least-mean-square

MAI: multiple-access interferences

MRC: maximum ratio combining

PCS: personal communication systems

RLS: recursive least-squares

SNIR: signal-to-noise-plus-interference ratio

SNR: signal-to-noise ratio

SMRC: space maximum ratio combining

SOPT: space optimum combining

TACS: total access communication system

TDMA: time-division multiple-access

TMRC: time maximum ratio combining

TOPT: time optimum combining

REFERENCES

1. F. Adachi, "Postdetection optimal diversity combiner for DPSK differential detection," *IEEE Trans. Vehicular Technology*, vol. 42, pp. 326–337, Aug. 1993.

2. R. T. Compton, Jr, *Adaptive Antennas*, Prentice Hall, Englewood Cliffs, NJ, 1988.

3. J. Dunlop and D. G. Smith, *Telecommunications Engineering*, Chapman & Hall, London, UK, 1994.

4. D. D. Falconer, F. Adachi, and B. Gudmundson, "Time division multiple access methods for wireless personal communications," *IEEE Communications Mag.*, vol. 33, pp. 50–57, Jan. 1995.

5. K. S. Gilhousen, I. M. Jocobs, R. Padovani, A. J. Viterbi, L. A. Weaver Jr., and C. E. Wheatley, "On the capacity of a cellular CDMA system," *IEEE Trans. Vehicular Technology*, vol. 40, pp. 303–312, May 1991.

6. K. S. Gilhousen, I. M. Jocobs, R. Padovani, and L. A. Weaver Jr., "Increased capacity using CDMA for mobile satellite communication," *IEEE J. Selected Areas in Communications*, vol. 8, pp. 503–513, May 1990.

7. G. H. Golub and C. F. V. Loan, *Matrix Computations*, The Johns Hopkins University Press, Baltimore, MD, 1983.

8. D. J. Goodman, "Trends in cellular and cordless communications," *IEEE Communications Mag.*, vol. 29, pp. 31–40, June 1991.

9. A. M. Haimovich, "Asymptotic distrbution of the conditioned signal-to-noise ratio in an eigenanalysis-based adaptive array," submitted to *IEEE Trans. Aerospace and Electronic Systems*, 1995.

10. A. M. Haimovich and Y. Bar-Ness, "An eigenanalysis interference canceler," *IEEE Trans. Acoustics, Speech, and Signal Processing*, vol. 39, pp. 76–84, Jan. 1991.

11. A. M. Haimovich and X. Wu, "Eigenanalysis based array processing for mobile communications," in *Proceedings of the 1994 Princeton Conference on Information Science and Systems*, Princeton, NJ, pp. 203–208, Mar. 1994.

12. S. Haykin, *Adaptive Filter Theory*, Prentice Hall, Englwood Cliffs, NJ, second ed., 1991.

13. N. Ishii and R. Kohno, "Spatial and temporal equalization based on an adaptive tapped-delay-line array antenna," in *Proceedings of the 1994 IEEE Personal Indoor and Mobile Radio Communications (PIMRC)*, The Hague, Netherlands, pp. 232–236, Sept. 1994.

14. P. Jung, P. W. Baier, and A. Steli, "Advantages of CDMA and spread spectrum techniques over FDMA and TDMA in celluar mobile radio applications," *IEEE Trans. Vehicular Technology*, vol. 42, pp. 357–364, Aug. 1993.

15. B. H. Khalaj, A. Paulraj, and T. Kailath, "Spatio-temporal channel estimation techniques for multiple access spread spectrum systems with antenna arrays," in *Proceedings of the IEEE International Conference on Communications (ICC)*, Seattle, WA, pp. 1520–1524, June 1995.

16. I. P. Kirsteins and D. W. Tufts, "Adaptive detection using low rank approximation to data matrix," *IEEE Trans. Aerospace and Electronic Systems*, vol. 30, pp. 55–67, Jan. 1994.

17. R. Kohno, "Spatial and temporal filtering for co-channel interference in CDMA," in *Proceedings of the IEEE Third International Symposium on Spread Spectrum Techniques & Applications (ISSSTA '94)*, Oulu, Finland, pp. 51–60, July 1994.

18. R. Kohno, H. Imai, M. Hatori, and S. Pasupathy, "Combination of an adaptive array antenna and a canceller of interference for direct-sequence spread-spectrum multiple-access system," *IEEE J. Selected Areas in Communications*, vol. 8, pp. 675–681, May 1990.

19. R. Kohno, R. Meidan, and L. B. Milstein, "Spread spectrum access methods for wireless communications," *IEEE Communications Mag.*, vol. 33, pp. 58–67, Jan. 1995.

20. W. C. Lee, "Overview of celluar CDMA," *IEEE Trans. Vehicular Technology*, vol. 40, pp. 291–302, May 1991.

21. J. C. Liberti and T. S. Rappaport, "Reverse channel performance improvements in CDMA cellular communication systems employing adaptive antennas," in *Proceedings of the IEEE GLOBECOM*, Houston, TX, pp. 42–47, Nov. 1993.

22. R. Monzingo and T. Miller, *An Introduction to Adaptive Arrays*, John Wiley, New York, NY, 1980.

23. A. F. Naguib and A. Paulraj, "Performance of CDMA cellular networks with base-station antenna arrays," in *Mobile Communications: Advanced Systems and Components, 1994 International Zurich Seminar on Digital Communications Proceedings*, Zurich, Switzerland, pp. 87–100, Mar. 1994.

24. J. G. Proakis, *Digital Communications*, McGraw-Hill, New York, NY, 1989.

25. D. J. Rabideau and A. O. Steinhardt, "Fast subspace tracking," *IEEE Trans. Aerospace and Electronic Systems*, vol. 10, pp. 853–863, Nov. 1994.

26. I. S. Reed et. al., "Rapid convergence rates in adaptive arrays," *IEEE Trans. Aerospace and Electronic Systems*, vol. 10, pp. 853–863, Nov. 1974.

27. M. V. S. Anderson, M. Millnert and B. Wahlberg, "An adaptive array for mobile communication systems," *IEEE Trans. Vehicular Technology*, vol. 40, pp. 230–236, Feb. 1991.

28. D. L. Schilling, L. B. Milstein, R. L. Pickholtz, F. Bruno, E. Kanterakis, M. Kullback, V. Erceg, W. Biederman, D. Fishman, and D. Salerno, "Boradband CDMA for personal communication systems," *IEEE Communications Mag.*, pp. 86–93, Nov. 1991.

29. G. W. Stewart, "An updating algorithm for subspace tracking," *IEEE Trans. Signal Processing*, vol. 40, pp. 1535–1541, June 1992.

30. S. C. Swales, M. A. Beach, and D. J. Edwards, "Multi-beam adaptive base-station antennas for cellular land mobile radio systems," in *Mobile Radio and Personal Commun. Conf.*, UK, pp. 341–348, Dec. 1989.

31. S. C. Swales, M. A. Beach, D. J. Edwards, and J. P. McGeehan, "The performance enhancement of multibeam adaptive base-station antennas for cellular land mobile radio systems," *IEEE Trans. Vehicular Technology*, vol. 39, pp. 56–67, Feb. 1990.

32. B. R. Vojcic, R. L. Pickholtz, and L. B. Milstein, "Performance of DS-CDMA with imperfect power control operating over a low earth orbiting satellite link," *IEEE J. Selected Areas in Communications*, vol. 12, pp. 560–567, May 1994.

33. J. H. Winters, "Optimum combining in digital mobile radio with cochannel interference," *IEEE Trans. Vehicular Technology*, vol. 33, pp. 144–155, Aug. 1984.

34. J. H. Winters, "Signal acquisition and tracking with adaptive arrays in the digital mobile radio system IS-54 with flat fading," *IEEE Trans. Vehicular Technology*, vol. 42, pp. 377–384, Nov. 1993.

35. J. H. Winters, J. Salz, and R. D. Gitlin, "Adaptive antennas for digital mobile radio," in *Adaptive Array Symposium*, Bethpage, NY, pp. 81–85, Nov. 1992.

36. J. H. Winters, J. Salz, and R. D. Gitlin, "The impact of antenna diversity on the capacity of wireless communications systems," *IEEE Trans. Communications*, vol. 42, pp. 1740–1751, Feb./March/April 1994.

37. X. Wu and A. M. Haimovich, "A simple projection based adaptive array with applications to mobile communications," in *Proceedings of the 1994 Adaptive Antenna Systems Symposium*, Melville, NY, pp. 37–42, Nov. 1994.

38. X. Wu and A. M. Haimovich, "Adaptive arrays for increased performance in mobile communications," to be presented at *The Sixth International Symposium on Personal, Indoor and Mobile Radio Communications (PIMRC'95)*, Sept. 1995.

39. X. Wu and A. M. Haimovich, "Space-time processing for CDMA communications," in *Proceedings of the 1995 Conference on Information Science and Systems*, Baltimore, MD, pp. 371–376, Mar. 1995.

40. Y.-S. Yeh and D. O. Reudink, "Efficient spectrum utilization for mobile radio systems using space diversity," *IEEE Trans. Communications*, vol. 30, pp. 447–455, Mar. 1982.